Improving Dynamic Performance in DC Microgrids Using Trajectory Control

by

Marco Andrés Bianchi

Ing., Universidad Nacional del Comahue, 2013

A THESIS SUBMITTED IN PARTIAL FULFILLMENT OF THE REQUIREMENTS FOR THE DEGREE OF

MASTER OF APPLIED SCIENCE

in

The Faculty of Graduate and Postdoctoral Studies

(Electrical & Computer Engineering)

THE UNIVERSITY OF BRITISH COLUMBIA

(Vancouver)

December 2017

Abstract

Direct-current (dc) microgrids interconnect dc loads, distributed renewable energy sources, and energy storage elements within networks that can operate independently from the main grid. Due to their high efficiency, increasing technological viability and resilience to natural disturbances, they are set to gain popularity. When load-side converters in a microgrid tightly regulate their output voltages, they are seen as constant power loads (CPLs) from the standpoint of the source-end converters. CPLs can cause instability within the network, including large voltage drops or oscillations in the dc bus during load transients, which can lead to dc bus voltage collapse. Traditionally, the stability of CPL-loaded dc microgrids relies on the addition of passive elements, usually leading to dc-bus capacitance increase. In this scenarios, source-end converters controllers are usually linear dual proportional-integral (PI) compensators. The limited dynamic response of these controllers exacerbates the CPL behavior, which leads to the use of larger passive elements. Recent contributions focus on implementing control modifications on the source-end converter in order to improve the system performance under CPLs. Particularly, the use of state-plane based controllers has been studied for the case of a single dc-dc power converter loaded by a CPL, showing fast and robust transient performance. However, the microgrid problem, where these faster converters interface with others of a slower response has not been studied thoroughly. This work proposes the use of a fast state-plane controller to replace one of the systems source-end converters controllers in order to improve three aspects of the microgrid operation: resiliency under CPL's steps, load transient voltage regulation, and voltage transient recovery time.

Since the converter is operating within a microgrid, the controller incorporates a traditional droop rule to enable current sharing with the rest of the converters of the network. The small-signal stability improvement of the whole system obtained by the addition of a single faster controller is analyzed for a linear model, and a parametric analysis demonstrates the improvements in a detailed model. Simulations and experimental results of a microgrid with three converters feeding a CPL prove the effectiveness of the technique for large-signal transients.

Lay Summary

Direct-Current (dc) microgrids are electrical grids that connect electrical loads and low power electrical energy sources through a dc bus. Power converters enable the power flow from the energy sources to the dc bus and from the dc bus to the loads. The speed at which a power converter reacts to source or load perturbations depends on its hardware and the controller in its firmware. When the combined speed of the load-side converters is similar or larger than that of the source-end converters the first one is seen as a constant power load (CPL) during perturbations. The CPL behavior is often mitigated with oversized hardware, which is a sub-optimal solution. This work proposes to replace the conventional controller in only one of the source converters with a faster trajectory controller. The new controller, which requires only firmware modification, mitigates the CPL behavior and expands the microgrids stable operating area.

Preface

This work is based on research performed at the Electrical and Computer Engineering department of the University of British Columbia by Marco Andrés Bianchi, under the supervision of Dr. Martin Ordonez.

A first version of this work was presented in IEEE 7th International Symposium on Power Electronics for Distributed Generation Systems (PEDG), 2016, [1], and later extended and in preparation for submission to IEEE Transactions on Power Electronics.

As first author of the above-mentioned publication, the author of this thesis developed the theoretical concepts and wrote the manuscripts, receiving advice and technical support from Dr. Martin Ordonez, and developed simulation and experimental platforms, receiving contributions from Dr. Ordonez's research team.

Table of Contents

List of Tables

List of Figures

Acknowledgements

I would like to thank my supervisor Dr. Martin Ordonez for recruiting me to be part of his research team. I am very grateful for his great enthusiasm, and his continuous support and commitment that made this learning experience so rich and fascinating.

I would also like to acknowledge my lab mates. Working with them along my program was a privilege and a beautiful adventure. Special thanks to my closest friends in Canada for encouraging and helping me when I needed it, and to my friends in Argentina for being in touch and making me feel they are close.

Finally, I would like to thank my parents Claudia and Roberto and my sister Mara, for their unconditional love and their faith in me.

To my family and friends.

Chapter 1

Introduction

1.1 Motivation

Microgrids are electrical networks that interconnect power energy sources with storage and consumption elements, and that can operate as a single controllable system. Their power range can vary from around 0-10 kW [2] up to 0-100 kW [3]. Their proliferation is a consequence of the increasing technological viability for integrating distributed renewable energy resources efficiently and reliably at a rapidly reducing cost. The nature of microgrids of being able to operate independently from the main electrical grid, makes them an appealing solution to supply the customer unmet demand in developing countries, which is currently of 1.2 billion people that do not have access to electricity [2]. Moreover, its resilience to natural disasters and other disruptions, and its capability of incorporating more carbon-efficient ways of producing and distributing energy have motivated an increased number of installations around the world.

It is expected that the rapid growth of dc-native loads will lead to the popularization of dc and hybrid ac/dc microgrids [4]. DC microgrids show high efficiency and enable the simple interconnection of renewable energy sources with loads and energy storage systems using a small number of power conversion stages. At a given instant a microgrid can be analyzed as a set of converters supplying energy from the sources to a dc bus, and another set of converters transferring energy from the bus to the loads. Because of the small scale storage elements, microgrids dynamics are faster than that of the traditional ac grid, which is subjected to the inertia of massive rotating electrical machines. Microgrids fast dynamics make these networks especially vulnerable to sudden changes in the operating conditions of the power converters interconnected within them. Particularly, when load-end converters tightly regulate their load voltage they behave as constant power loads (CPL), which dynamic effect emulates a variable negative resistance and challenges the microgrid's stability. A microgrid including a CPL load can be modeled as a set of parallel converters supplying energy to dc bus where a single CPL is connected that simulates the combination of all the electronic loads [5–7]. The most critical-scenario, from the dc bus stability standpoint, happens when an instantaneous power mismatch between sources and loads leads to a sudden voltage change in the bus capacitors. During sudden transients, which could be the result of a load step or a converter turnoff, the effects of both fast and slow system dynamics can be identified in the dc voltage signal[8]. While fast dynamics can be directly linked to the converters' voltage controllers, the slower transients are imposed by the droop controllers and the interaction among them. Several contributions have focused on improving the droop dynamics, analyzing the system's long-term behavior and neglecting the fast dynamics during transients [9, 10]. However, the mitigation of the negative effects of CPL transients, such as voltage drop and oscillation, requires the fast dynamics of the system to be addressed. A number of strategies have been studied in the literature that aim to mitigate the CPL behavior. From the wide range of possibilities, including passive damping, and the application of advanced control techniques, the use of state-plane based control schemes in source-end converters can result in very fast and robust performance during sudden transients, which is of particular interest to increase the resilience of microgrids. Although, these techniques have been implemented in power converters connected to CPL's, the effect of their use in the source-end converter of a microgrid have not been studied extensively. Moreover, some contributions in the literature looked to improve the microgrid resilience under transients by implementing faster controllers in some of the converters of the microgrid. These works, where dissimilar speed converters can be found, are mostly restricted to hybrid energy storage applications. Furthermore, the converters' inner control techniques employed are conventional linear techniques, which are known for having a limited dynamic response. Applying a faster control technique in only some of the converters of a microgrid to increase the system resilience is an appealing concept when the challenge of improving the pre-existing infrastructure's dynamic performance is needed. This work proposes to replace one of the conventional controllers in one of the power converters of a microgrid with the faster state-based one in order to improve the system resilience and its dynamic performance under sudden CPL transients.

1.2 Literature Review

The behavior of CPL's was extensively discussed in the literature and many strategies have been studied that aim to mitigate its negative effect on the stability of the system. While some of the proposed techniques are designed for its application in dc microgrids, other works focus on systems comprised of a single-converter connected to a CPL. The adaptation of the techniques employed to improve the dynamic performance of stand-alone converters for their use in microgrids is often possible, and can potentially motivate new ideas. The universe of techniques that tackle the CPL challenge can be grouped in three main categories, depending on the element of the microgrid where these are applied, and are shown in Fig. 1.1. Firstly, external stabilizers (❶ in Fig. 1.1) add new devices to the network, usually passive elements, with the sole purpose of stabilizing the system. Secondly, load-end converters stabilizers (❷ in Fig. 1.1) implement the stabilization as part of the load converter control law. Finally, a third group of techniques implement the stabilization techniques whithin the source-end converter's controllers (❸ in Fig. 1.1). The next three sub-sections will cover the mentioned main contributions categories that are found in the literature.

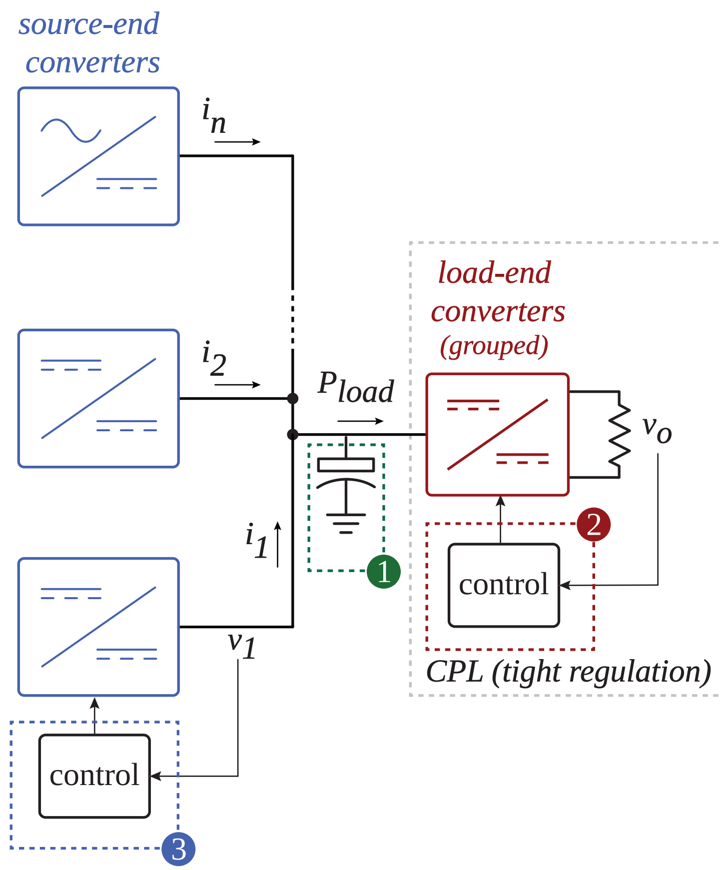

Figure 1.1: Diagram of a microgrid showing the three categories of techniques used to mitigate the CPL negative behavior of the system. The stabilization techniques are grouped according to the element of the microgrid where they are applied: addition of new elements to the network (❶); load-side converters' controllers (❷), source-end converters' controllers (❸).

1.2.1 Passive and Active Damping Using Additional Circuitry

The techniques that stabilize the CPL negative behavior using circuitry that is external or additional to the source-end and load-end converters (❶ in Fig. 1.1) can be separated in active and passive damping stabilization. External active damping relies on the use of additional power electronics to increase the damping of the circuit. A bidirectional buck-boost converter in parallel to the dc bus is usually employed, whose current controller is shaped to emulate the behavior of a resistive load or an *RC* branch connected to the bus [11–14]. While some of the proposals re-circulate the absorbed energy to a neighboring dc bus comprised of batteries or super-capacitors, other topologies need to deal with zero net energy since they only count with a regular capacitor to store energy.

On the other hand, passive damping mitigates the CPL behavior with the addition of networks of passive elements or the re-sizing of the source-converters output filters . The external passive dampers include RL and RC arrays that connect to the converters output filters or the dc bus [15]. Alternatively, when re-sizing converters LC output filters, two main approaches are possible: decreasing the filter series inductor values or increasing the output capacitor [16]. Because a decrease in the inductance deteriorates the converter's electromagnetic compatibility, the over-sizing of the output capacitors is usually preferable and is a common practice to improve the system stability.

In general, in both active and passive methods, the damping impedance is determined by the application of Routh-Hurwitz's or Middlebrook's criterion [17]. The stability criterion requires a linear model of the system to be obtained, which is usually done considering the open-loop transfer functions of the source-end power converters and the linear model of the non-linear load under certain load conditions.

The use of active damping techniques exhibits a larger level of complexity than that of passive stabilization. However, its application could be desirable in high power systems where having non-dissipative dampers could signify a large reduction in energy consumption. On the other hand, passive stabilization particularly by resizing the dc bus capacitance can be an appealing solution because of their simplicity but it also increases the size and cost of the microgrid building blocks.

1.2.2 Load-End Converters Stabilizers

These stabilizers constitute a family of solutions that increase the system stability by implementing control strategies embedded in the load-end converters (❷ in Fig. 1.1). Their control law aims to limit the maximum rate at which the load-end converter input current can change. Consequently, the CPL behavior is mitigated at the expense of a slower load voltage dynamic regulation. In [18], this method is implemented by emulating a virtual capacitance of the dc bus for a single CPL, and in [19] this is done using stabilizing agents for a number of parallel load-end converters. The stabilizers decrease the converters input power reference as a function of the high-frequency components of the square of the input voltage signal. The objective is for the load-side converter its CPL behavior during transients. On the other hand, [20] proposes to implement a virtual impedance emulated at the input of the CPL converter. The impedance, which can be emulated in series or in parallel, is mathematically defined using a piecewise function, that gives the impedance a different behavior depending on the frequency. In this way, the impedance stabilizes the system at the frequencies where the Middlebrook's criterion is not originality met, but his behavior is null outside of this frequency scope. A different approach is studied in [21], where the CPL controller maximum current saturation values are theoretically determined as a function of the source-end converters limitation. The paper establishes a simple rule that should be followed when configuring the CPL controller's operating limits in order to guarantee stability in start-up and step-up transients.

Load-end converters stabilizers are an interesting approach that tackles the challenge of the CPL behavior by decreasing the fast dynamic response of the load-end converters. However, this is expected to be detrimental to the load voltage regulation and is undesirable for many cases.

1.2.3 Source-End Converters Stabilizers

The described methods so far mitigate the negative behavior seen in CPL-loaded microgrids with methods that do not require any modification of the control law of the controller of the source-end converter. In these cases, source-end converters are traditionally controlled using conventional linear control techniques. Particularly popular is the use of current-mode dual proportional-integral compensators (PI)[22, 23]. In these control schemes, the existence of a current-loop simplifies the voltage control and provides safety benefits, but imposes the bandwidth reduction of the outer voltage loop. Consequently, dual PI ruled converters dynamic performance tends to be slow, which exacerbates the negative effects of the CPLs in the microgrid.

On the other hand, the application of source-end controllers specifically designed to mitigate the CPL behavior (❸ in Fig. 1.1) covers a wide range of options: linear, mixed and non-linear techniques. Linear approaches focus on stabilizing the small-signal closed-loop transfer function using linear feedback control. In [5, 24–26] this is done by the application of active damping techniques, while in [16] it is done using passivity-based control. Alternatively, a linear modification of the current sharing controller in the source-end converters of hybrid energy storage systems (HESS) was studied recently to improve the dynamic performance of dc microgrids [27–29]. The inner control law of the source-end converters is a conventional dual loop PI compensator. But, the external current sharing controller is modified to produce a transient response that is coherent with the discharge time of the energy storage technology that the converter is interfacing. With this strategy, converters connected to super-capacitors will respond faster than those connected to batteries, providing a higher frequency current pulse that should extinguish after the transient is over. Although its application is specifically designed for HESS scenarios, the concept of having a few converters ruled by a faster control law with the objective of improving the microgrid stability for a more general application was not studied extensively in the literature.

A number of controllers combine the application of non-linear operations with linear control techniques. These controllers achieve better transient performance while keeping the simple implementation of classic linear control theory. In [30] and [31] an outer voltage loop is used in combination with a hysteresis current control and peak current control respectively. Another hybrid controller is introduced for different converter topologies in [32–34], where a non-linear geometric loop regulates the voltage and a conventional inner PI controls the inductor current, although in these cases the converter is not loaded with a CPL. Moreover, adaptive controllers like in [35] also enable the application of linear techniques by estimating the parameters of the system and modifying the linear compensator's gains in real time. In [36, 37] a non-linear state feedback loop is employed in order to obtain a large-signal linearized plant that is then compensated applying conventional linear techniques. Other studies apply less traditional but faster controllers after a nonlinear feedback transformation is performed, at the cost of increased mathematical complexity. In [38], the nonlinear transformation is followed by a proportional state feedback which gain array is obtained by the Ackerman's formula for poles allocation; while in [39], the nonlinear feedback takes the system to a canonical form that enables the application of a backstepping method to obtain the control law. Both methods implement state variables observers in order to increase the control immunity to parameters mismatch. Among non-linear control techniques, boundary controllers have demonstrated very good performance while ruling the behavior of the converter during sudden load changes. Since these controllers do not experience the bandwidth limitation of conventional linear, and hybrid controllers, they can make the converter work closer to the theoretical limit, studied in [40], and its implementation does not require complex mathematical operations. First order sliding mode controllers were studied in [41, 42] for their use in CPL loaded converters, and the natural trajectories derived in [43, 44] were applied in the control laws of a power converter with a CPL in [45]. While state-plane controllers display rapid dynamic response, the work described above focuses on one converter only (stand-alone), rather than the multiple converters interacting in a dc microgrid; the interaction of a fast state-plane ruled converter with other conventional converters in a microgrid is yet to be studied.

1.2.4 Summary

The presence of CPLs in dc microgrids imposes an instability challenge that has been tackled using three main approaches: use of additional stabilizing circuitry, modification of the load-side converter' controller, and modification of the source-end converter' controller. The published work succeeds on improving the dc microgrid performance under CPL behavior but there are still areas that can be explored. In particular, the use of faster state-based controllers embedded in the source-end converters of a microgrid while interacting with other conventional slower controllers in a microgrid is lacking in the literature. The use of dissimilar speed controllers in a dc microgrid is mostly limited to the specific case of hybrid energy storage systems, and its study for a more general case is yet to be done. These technical challenges are addressed in this thesis and a new dc microgrid stabilization approach is proposed.

1.3 Contribution of the Work

This work presents a novel stabilization approach that mitigates the negative effects of CPLs in a dc microgrid by implementing a faster controller in one of the converters and studies the implications of having a faster controller in the system. The contributions of this thesis are summarized below:

- A state-trajectory controller with an embedded droop law is designed and assessed for its implementation in one of the source-end converters of a dc microgrid. The proposed approach improves three critical aspects of the microgrid operation: 1) resiliency under large CPL's steps; 2) load transient voltage regulation; 3) voltage transient recovery time. The strategy does not require to update all the controllers of the microgrid, and the improvements in the performance are obtained by only implementing the controller in a single source-end converter. Figure 1.2 shows a conceptual comparison between the proposed and traditional strategies. The proposed controller (case A) leads to dynamic performance improvements under the sudden load change (CPL) when compared to traditional dual PI current-mode controllers (case B).

- The implications of having a faster controller in one of the source-end converters of the dc microgrid are studied. It is shown that having faster controllers will improve the small-signal stability of the system. Moreover, the existence of a tradeoff between droop dynamics and dc bus dynamic regulation is observed when one of the parallel converters is faster.

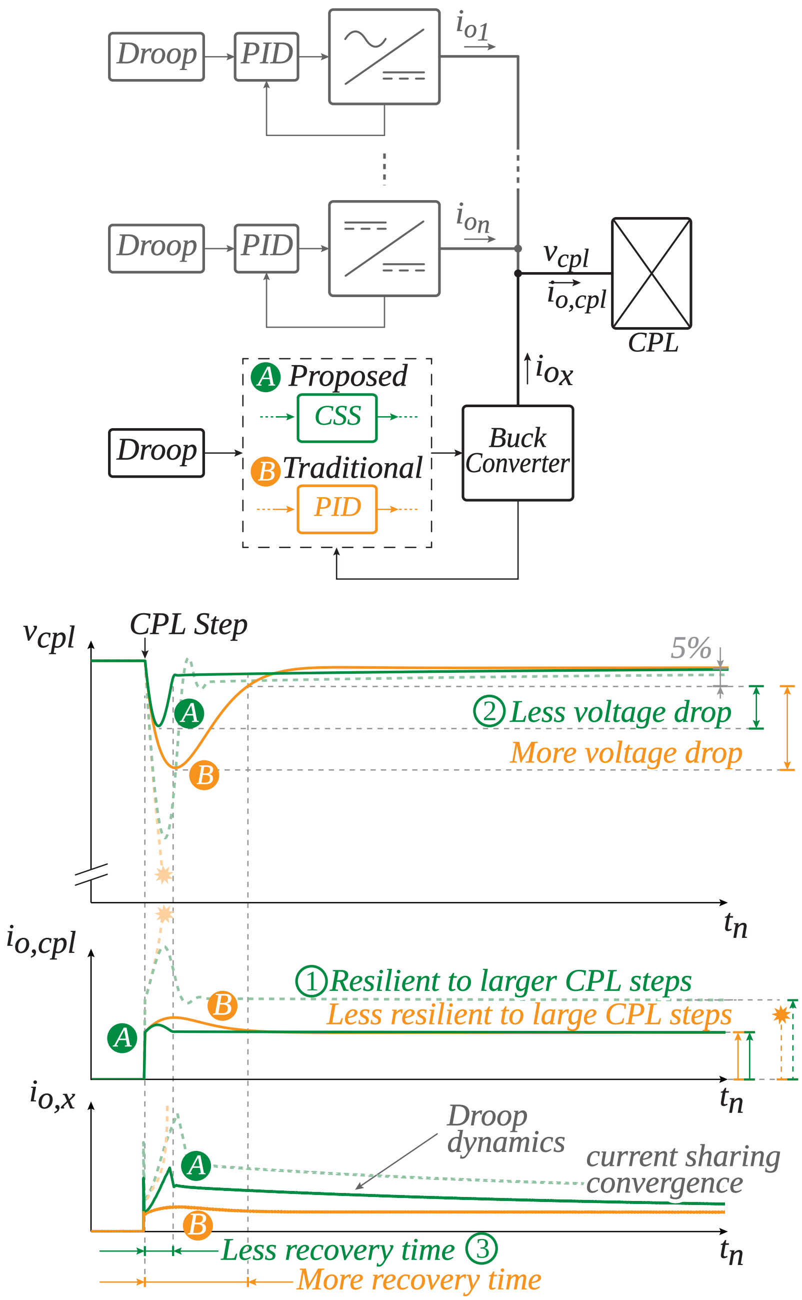

Figure 1.2: A dc microgrid comprising several parallel converters connected to a CPL. Its dynamic performance is depicted for the traditional approach (B) versus the proposed approach (A), where a traditional linear control is replaced with a CSS controller in one of the source-end converters). Case A improves three aspects of the microgrid operation: resiliency to CPL steps ①, transient voltage regulation ②, transient recovery time ③. In case A, $i_{o,x}$ takes a larger share of $i_{o,cpl}$ during the transient, what results in a faster dynamic regulation of v_{cpl}. The current imbalance after the transient for case A slows down the droops dynamics, however, the current sharing capability is maintained.

1.4 Thesis Outline

The present work is organized as follows;

- In Chapter 2, the behavior of a CPL when connected to a power converter with an *LC* output characteristic is explained. The ON state trajectories of a normalized version of this system are obtained for a range of initial conditions and CPL steps, and the maximum stable power step is found. Then, the results obtained for a single power structure are extended for the case of parallel source-end converters in a microgrid.

- In Chapter 3, the small-signal stability of a linearized model of the system is studied when one of the converters is ruled by a faster controller. And the tradeoff for the proposed strategy between current sharing dynamics and dynamic voltage regulation is also explained. The different speed controllers are modeled using dual PI compensators, and the practical limitations of expanding the bandwidth of these converters are discussed.

- Chapter 4 derives and explains the control law to be used, and the proposed strategy explained for the stand-alone and microgrid cases in the state-plane domain.

- In Chapter 5 the concept is assessed using a microgrid simulation model. And a more comprehensive description of the system performance of the proposed approach versus that of the traditional approach is obtained through a parametric analysis for a normalized microgrid.

- Experimental results of a microgrid composed of three power converters feeding a CPL prove the validity of the concept in Chapter 6. When one of the controllers ruling one of the power converters is replaced with a CSS controller with embedded droop, the dynamic performance of the dc microgrid improves, showing less voltage drop, and faster responses during load transients.

- Finally, in Chapter 7 a summary and conclusions of this work are presented, along with some details of future research ideas.

Chapter 2

Constant Power Load Behavior And Maximum Power Step

In this chapter, the behavior of a system comprising power converters loaded with a constant power load is studied. The buck topology is a common structure found in dc microgrids and will be used as source-end converter. It is observed that for a given initial condition, there is a theoretical maximum load power step-up (ΔP_{crit}) that the system can withstand before the dc voltage collapses. Stable power steps that are close to ΔP_{crit} are possible if the control law ruling the buck converter reacts immediately after the step occurs. First, the value ΔP_{crit} is obtained for a normalized system and sets a maximum limit against which the performance of any control law can be compared to characterize its large signal behavior. The analysis is later extended from the case of a single converter to several power converters in a microgrid.

2.1 Single Buck Converter Case

In order to add generality to the present work, the analysis will be performed in a normalized domain when possible. The normalization base values are given by the filter's characteristic impedance and time constant, and the power supply input voltage of the buck converter. When the system includes more than one converter, the base values will be obtained from the parameters of one of them. This procedure makes the study independent of the specific filter and voltage settings. In Figure 2.1 a schematic of a normalized buck converter connected to

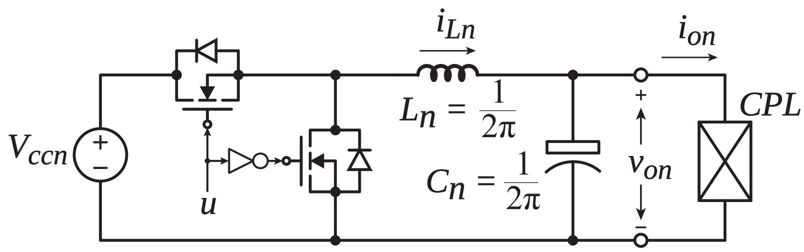

Figure 2.1: One buck converter, as the ones found in microgrids, connected to a constant power load (CPL). Variables and parameters are normalized using the power supply input voltage (V_{cc}) and the LC output filter resonant frequency (F_0) and impedance (Z_0) as normalization base values. This is indicated using the subscript "n".

a CPL is depicted. The parameters and variables names have the subscript "n" to indicate that the respective quantities have been normalized. The normalization for values of voltage V_x, current I_x, impedance Z_x, or time T_x is performed as follows:

$$V_{xn} = V_x/V_{ref}, \qquad I_{xn} = I_x \cdot Z_0/V_{ref}, \qquad Z_{xn} = Z_x/Z_0, \qquad T_{xn} = T_x/T_0,$$

where the normalization base quantities are given by:

$$V_{ref} = V_{cc}$$

$$T_0 = 1/F_0 = 2\pi\sqrt{LC}.$$

In particular, the normalized values of the inductance and capacitance are obtained from the normalization of $Z_0 = \sqrt{L/C}$ their respective reactances using the impedance base quantity Z_0. The equations are:

$$L_n = L\frac{1}{T_0 Z_0} = \frac{1}{2\pi} \tag{2.1}$$

$$C_n = C\frac{Z_0}{T_0} = \frac{1}{2\pi}. \tag{2.2}$$

Using the normalized values, the current through the ideal CPL in Fig. 2.1 is given by:

$$i_{on} = \frac{P_{on}}{v_{on}}, \tag{2.3}$$

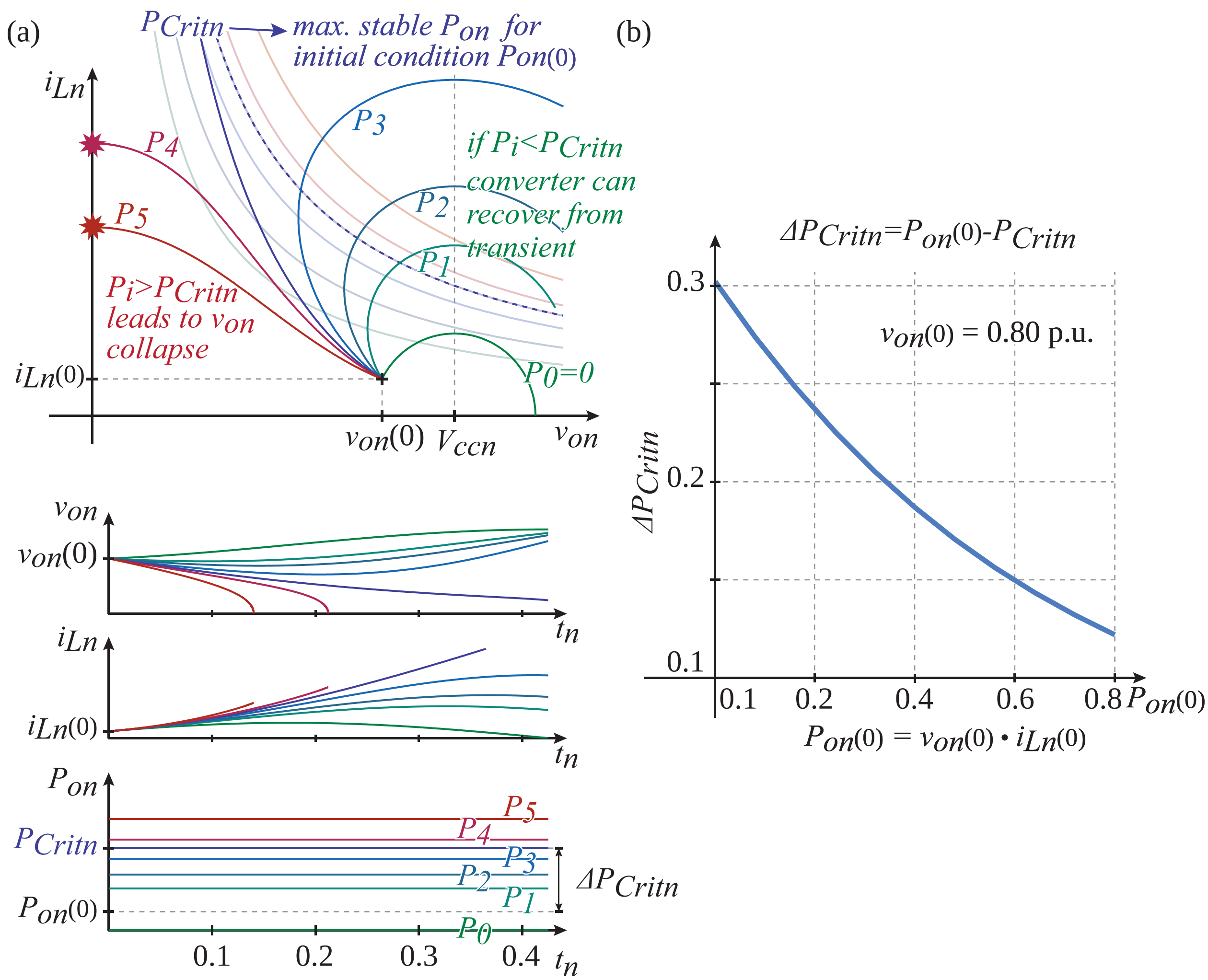

Figure 2.2: Behavior of a buck converter under constant power loads steps. (a) ON trajectories in both state-plane and time domain for a buck converter loaded with a CPL. For any set of initial conditions, there is a maximum stable power step value $\Delta P_{Critn} = P_{Critn} - P_{on}(0)$, where P_{Critn} is the CPL power after the step and $P_{on}(0)$ is the initial power. If the power after the step is smaller than P_{Critn} the system can recover from the transient keeping the ON a move to the new target point by adopting right switching actions. For values of power larger than the critical the system is unstable independently on the switching actions taken. (b) Normalized maximum stable power step ΔP_{Critn} vs. converter initial power $P_{on}(0)$. The value of ΔP_{Critn} when $P_{on}(0) = 0$ is approximately 0.3 p.u. for a normalized buck converter.

where P_{on} is the normalized load power. The dynamic behavior of the CPL can be understood from its small-signal resistance:

$$\frac{dv_{on}}{di_{on}} = -\frac{v_{on}^2}{P_{on}} = -r_{cpln}. \tag{2.4}$$

The negative incremental resistance introduces instability into the system, which may lead to dc voltage collapse if not compensated on time. Its destabilizing effect can be understood during a load step-up, which is the most challenging condition for a converter feeding a CPL occurs. At that moment, r_{cpln} decreases instantaneously. The consequent sudden increase of i_{on} tends to discharge the dc bus capacitor, leading to a decrease of v_{on}. This further decreases r_{cpln} and the process continues. If the inductor current i_{Ln} does not grow fast enough to compensate for the rapidly increasing i_{on} before the dc-voltage is too small, the transient could lead to a dc-voltage collapse. Therefore, the converter supplying the CPL should be fast enough for v_{on} to recover before r_{cpl} becomes too small. The maximum response speed that the converter can achieve is given by its reactive components, and at the same time limited by the effectiveness of the control technique ruling the converter.

Right after a CPL step-up, an optimal control law would make the buck converter adopt its ON structure ($u = 1$) since that would lead to an immediate increase of i_{Ln}. Figure 2.2(a) shows the converter's ON trajectories in the state-plane and the respective time domain responses for different power steps. For a given initial power $[v_{on}(0); i_{Ln}(0)]$, the converter follows different trajectories that vary with the power value after the step, which is called P_i with $i = 0, 1, 2, ...$ If the power after the step is lower than a critical value P_{Critn}, the trajectories move the operating point closer to the new target point, which will be at $v_{on}(0)$ but at a different current i_{Ln} that depends on the power step. In these transients, marked in the figure as P_0, P_1, P_2, and P_3, if the correct switching actions are taken, the converter can recover from the transient and reach the target value. While for the trajectories with final power P_1, P_2, and P_3 the load increases its power after the step, the ON trajectory marked as P_0 corresponds to a step-down. A negative power step is less challenging because r_{cpln} increases instantaneously after the step and so does the dc voltage.

It is observed that, the larger the power step, the larger the voltage drop on v_{on} and the longer it takes for the converter to recover. For each initial condition, there is a maximum power step final value that the converter can withstand, marked as P_{Critn} in the figure. If it is exceeded, the voltage collapses irreconcilably as shown for the cases P_4 and P_5 in which the trajectories reach the vertical axis ($v_{on} = 0$). This value defines a hardware limitation for the maximum power step that can be applied to the system. For lower P_i values, the use of an effective control technique can lead to an stable operating condition after the load step transient.

The value of P_{Critn} was calculated numerically for a number of initial conditions using MATLAB. The range of current values $i_{Ln}(0)$ was selected from 0 p.u. to 0.8 p.u while the voltage initial condition was set to $v_{on} = 0.8$ p.u., which will be the operating point for the cases studied in this work. The code implemented solves numerically the ON differential equations of the normalized buck converter (see (4.2) and (4.3)) for each set of initial conditions and for a given CPL step initialization value. Then, the resulting trajectory is marked as 'unstable' or 'stable', depending on whether or not it leads to a voltage what leads to the calculation of a new CPL power value. The process is iterated for different power values and P_{Critn} is found using successive approximations.

The results are summarized in Figure 2.2(b), as a function of the initial power $P_{on}(0) = 0.8 \cdot i_{Ln}(0)$ and the power step value $\Delta P_{Critn} = P_{Critn} - P_{on}(0)$. The chart shows that a buck converter can ride through a maximum ΔP of around 0.3 p.u. when initialized at zero P_{on}, and its capability decreases as $P_{on}(0)$ increases.

It is expected that a fast compensator will bring the converter close to its physical limit, allowing the system to withstand maximum load steps that are closer to ΔP_{Critn}. The results summarized in Fig. 2.2(b) can be used as a benchmark to compare the performance of any controller with the theoretical limit when the converter is subjected to CPL load step-ups. As the values in the curve correspond to a normalized buck converter, they can be extended to any converter after its parameters have been normalized.

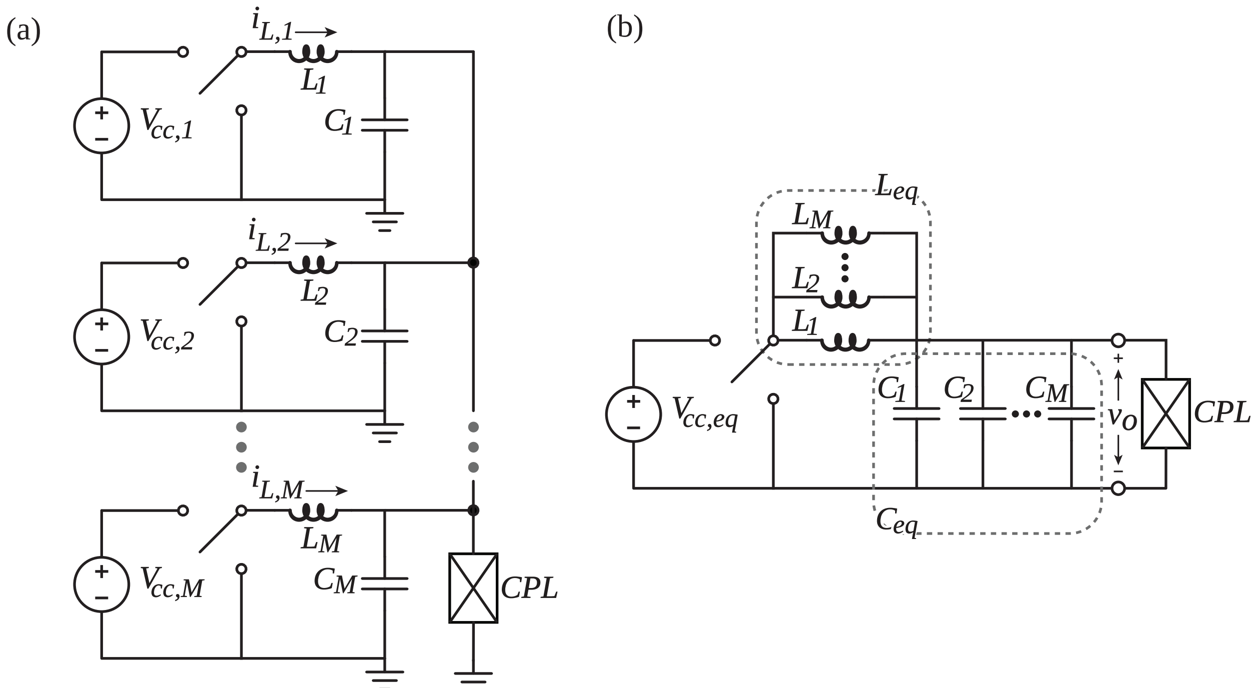

Figure 2.3: (a) M parallel buck converters in a microgrid supplying a CPL. (b) Microgrid equivalent single converter model for synchronized ON or OFF actions.

2.2 Multiple Buck Converters in a DC Microgrid

In a dc microgrid, the number of buck converters supplying the CPL is larger and the system can be represented as in Fig. 2.3(a). In order to extend the analysis to account for multiple converters, the parallel buck converters can be combined into a single equivalent unit. The maximum possible power step that the system can withstand, is obtained for the case in which the M converters have synchronized switching actions. For this scenario, the equivalent inductance L_{eq} and capacitance C_{eq} can be obtained by paralleling the individual elements of each converter.

$$L_{eq} = L_A \parallel L_B \parallel ... \parallel L_M \tag{2.5}$$

$$C_{eq} = C_A + C_B + ... + C_M \tag{2.6}$$

To obtain the input voltage of the equivalent circuit some extra steps are needed. The differential equations of the inductor current for the m-th converter and for the equivalent circuit are:

$$\frac{di_{L,m}}{dt} = \frac{1}{L_m}\left(V_{cc,m} - v_o\right) \tag{2.7}$$

$$\frac{di_{L,eq}}{dt} = \frac{1}{L_{eq}}\left(V_{cc,eq} - v_o\right). \tag{2.8}$$

If the total current through the equivalent inductor is $i_{L,eq} = \sum_{m=1}^{M} i_{L,m}$, then (2.8) can be rewritten as:

$$\sum_{m=1}^{M} \frac{di_{L,m}}{dt} = \frac{1}{L_{eq}}\left(V_{cc,eq} - v_o\right). \tag{2.9}$$

Finally, substituting (2.7) in (2.9) and solving for $V_{cc,eq}$:

$$V_{cc,eq} = L_{eq} \sum_{m=1}^{M} \frac{V_{cc,m}}{L_m}. \tag{2.10}$$

The equivalent circuit is depicted in Fig. 2.3(b), where L_{eq} and C_{eq} are the result of paralleling the converters' inductances and capacitances. Now, using the equivalent buck converter, the theoretical maximum power step that the system could withstand (ΔP_{Critn}) can be calculated from the results obtained for a single buck converter in Fig. 2.2(b). The normalizing power of the equivalent circuit is obtained from the normalizing base values $V_{ref} = V_{eq}$ and $Z_o = \sqrt{L_{eq}/C_{eq}}$ as shown below:

$$P_{ref} = \frac{V_{ref}^2}{Z_o} = V_{eq}^2 \cdot \sqrt{\frac{C_{eq}}{L_{eq}}} \tag{2.11}$$

Then, the critical power step-up for a given initial power $P_{on}(0)$ is defined by:

$$\Delta P_{Crit} = \Delta P_{Critn} \cdot P_{ref}, \tag{2.12}$$

where ΔP_{Critn} is obtained from the curve in Fig. 2.2(b). The value of ΔP_{Critn} obtained for a microgrid with parallel buck converters loaded by a CPL gives a theoretical limit of the maximum power step-up that can be applied in the system. As in the case of a single converter, it can be used to contrast the performance of the system against the ideal case, and measure the margin for improvement.

2.3 Summary

In this chapter, the incremental resistance of a CPL was derived and its implications on stability were discussed for a buck converter loaded by a CPL. The large-signal behavior of the system during load step-up transients was analyzed using the state-plane domain representation. Moreover, the maximum power step that the system can recover from (ΔP_{Crit}) was obtained for a range of initial power conditions for a single buck converter, and the results were extended for the microgrid case. ΔP_{Crit} can be used as a benchmark to observe how close the maximum stable power step of a given system is to the theoretical maximum, and measure the transient performance of the source-end converters controllers. The analysis was done in the normalized domain, and the normalization process was introduced. This allows the results to be extended to any problem that shares the same circuit topologies.

Chapter 3

Faster Source-End Converter Controllers in a DC Microgrid

The use of faster response control techniques in power converters with constant power loads should lead to an improvement in the system stability. Since CPL behavior is a consequence of the load-end converter being faster than the source-end one, an increased transient response of the latter should mitigate the negative CPL effects. Moreover, if the faster controller replaces one of the regular compensators in a microgrid with parallel converters loaded with a CPL, the stability of the system as a whole could be potentially improved. The inclusion of a faster compensator in the system increases the speed at which the combined set of parallel sources supplies power to the dc bus, and decreases the difference in the transient response between source converters and CPL.

When the converters are controlled using linear compensators, the dynamic response can be enhanced if the compensator's bandwidth is increased. However, this requires a proportional increase in switching frequency to prevent non-attenuated switching harmonics to be amplified by the compensator. Usually, an increase in switching frequency is undesirable since it moves the hardware out from the operating point it was designed for. Although traditional linear compensators exhibit a very limited response for a given switching frequency when compared with other non-linear strategies as state-plane based controllers, they can be used to model the microgrid behavior effectively. In particular, the effects of having a faster source-end controller in a microgrid is of interest in the present work.

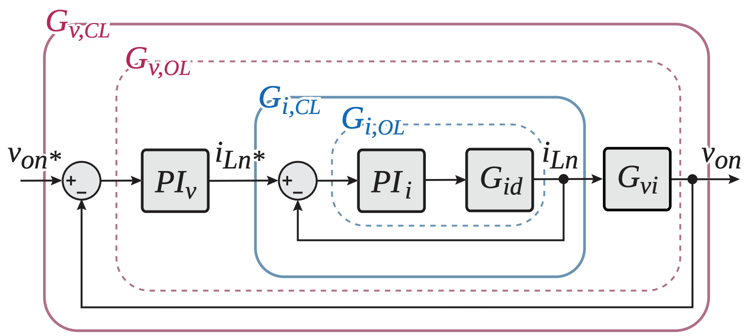

Figure 3.1: Nested dual loop control scheme: an inner PI loop controls the converter inductor current (i_{Ln}), while an outer PI loop controls the capacitor voltage (v_{on}).

This chapter first reviews some of the features of a traditional dual loop PI controller, which will be used later to model the source-end converters controllers in a microgrid. Secondly, a state-space model approximation of a system comprising a number of converters in parallel is derived and the small-signal stability of the model is then analyzed. The analysis is performed for the case in which one of the converters is controlled using a faster compensator than the others. Finally, section 3.3 assesses the large-signal behavior for a three parallel converter system with dissimilar controller speeds.

3.1 Traditional Controllers: Nested Dual Loop PI

A traditional control scheme for power converters involves using a nested dual loop PI compensator to control both current and voltage, as depicted in Fig. 3.1. The outer voltage loop is tuned to have a slower response than the inner current loop, which can be observed when comparing the bandwidths between both closed-loop Bode plots. Figure. 3.2 (b), depicts the voltage and current closed-loop frequency responses for a normalized buck converter compensated with a nested dual PI. The current compensator was tuned to achieve a crossover frequency f_i approximately 10 times lower than the switching frequency f_{sw}. The distance between f_i and f_{sw} gives enough room for the switching harmonics to be attenuated by

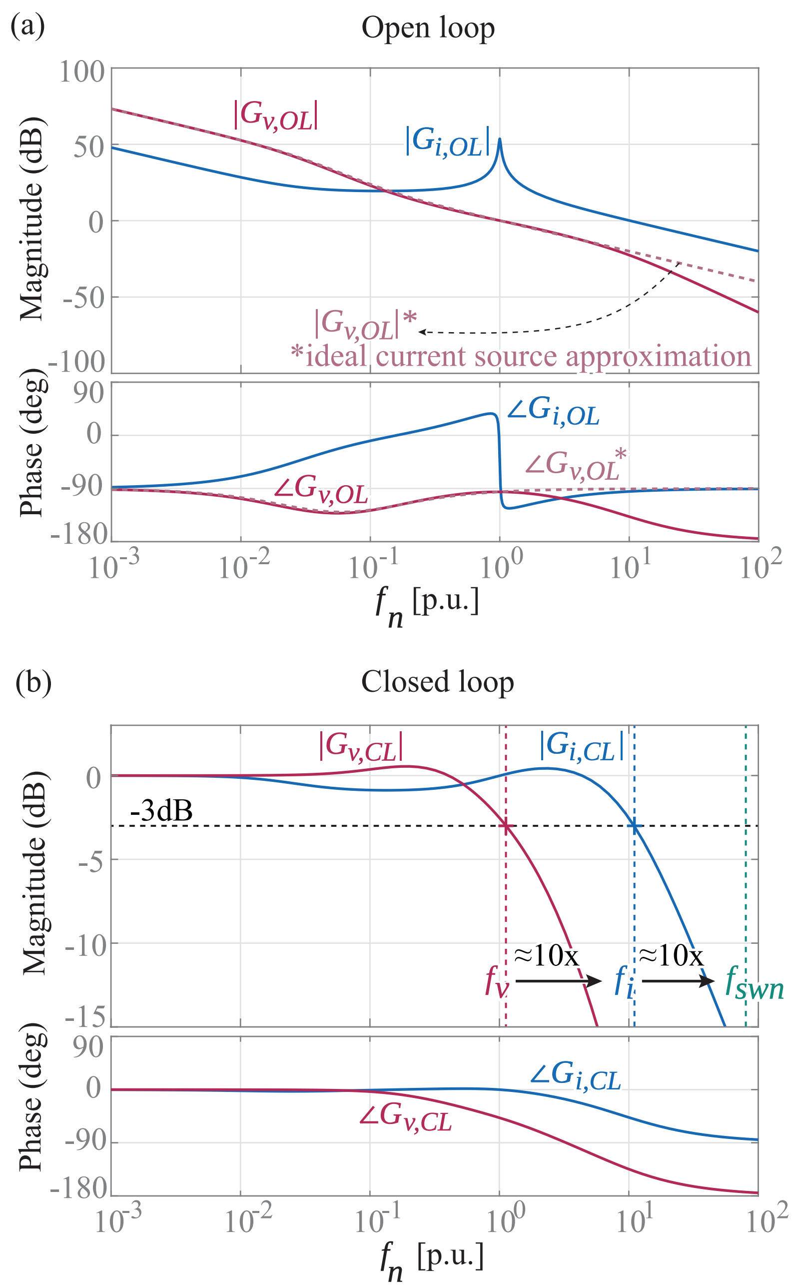

Figure 3.2: Normalized Bode plots of the control loops for a buck converter in light load condition. (a) shows the open loop Bode plots for both current ($G_{i,OL}$), and voltage ($G_{v,OL}$) loops. $G_{v,OL}*$ is the open loop frequency response when the current closed-loop is approximated with a constant current source. The approximation is accurate for a range that exceeds the closed-loop cut-off frequency. (b) Shows the closed-loop Bode plots and the separation required for cross-over frequencies, and with respect to the switching frequency.

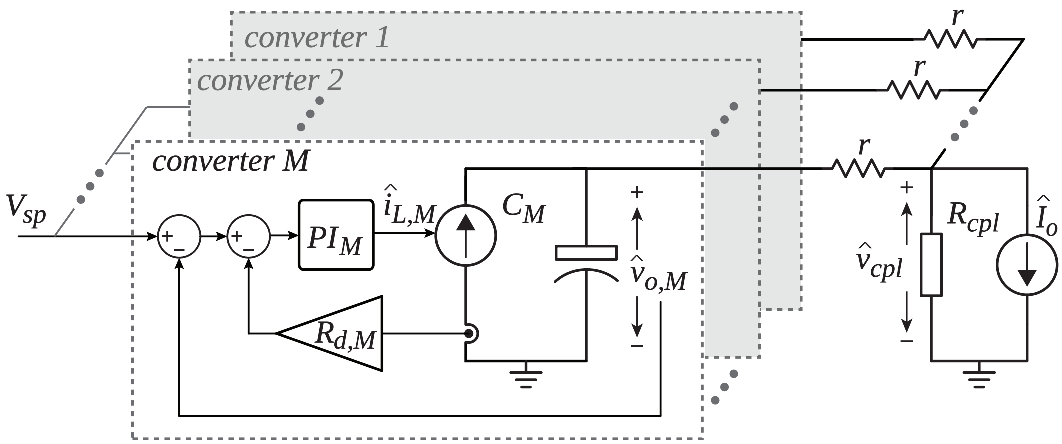

Figure 3.3: Linearized model for M parallel buck converters controlled using nested dual PI compensators. Since the dynamics of the inner current closed-loop are very fast in comparison with the voltage loop, the current loop behavior can be emulated using a controlled current source.

the compensator's low pass filter response, preventing the switching ripple to be amplified through the feedback loop [46, 47]. On the other hand, the voltage compensator closed-loop crossover frequency f_v is close to 10 times lower than that of the current compensator [47]. The separation between f_i and f_v makes the inner loop fast from the point of view of the voltage loop. Consequently, the dynamics of the current loop can be neglected when analyzing the behavior of the whole system, what leads to a lower order representation of the system. In Fig. 3.1, this is done by replacing the current closed-loop transfer function $G_{i,CL}$ with a unity gain, which is equivalent to replacing the current loop with a controlled current source. In Fig. 3.2, it is observed that the open loop Bode for the voltage compensator and plant when the current source approximation is used ($G_{v,OL}*$), matches that of the complete system representation ($G_{v,OL}$) for the frequency range of interest. The approximation $G_{v,OL}*$ deviates from $G_{v,OL}$ for frequencies where the response attenuation is already large enough, around -20 dB for the example in Fig. 3.2(a).

The described compensator constitutes a traditional control approach and will be employed in this chapter to model the behavior of a microgrid when one of the source-end controllers has increased speed. In the following chapters, it will be used to compare the microgrid dynamic performance of the proposed approach with that of the traditional approach.

3.2 Parallel Converters Linear Model Derivation and Small-Signal Stability

The effects on stability of having a single faster controller in one of the source-end converters of a microgrid can be studied modeling the compensators dynamics with a traditional nested dual loop PI controller. Because of the bandwidth separation between inner and outer closed-loops, the inductor dynamics in each converter can be neglected to obtain a reduced order system representation. The inner closed-loop can be modeled with a current source which operating point is set by the PI voltage compensator. Moreover, since the converters will share the load current in a microgrid the target voltage v_o^* in each of them will be set using a conventional droop law [48]:

$$v_o^* = V_{sp} - i_o \cdot R_d \tag{3.1}$$

where V_{sp} is the reference voltage at no load, i_o is the converter output current, and R_d is the droop resistance. If a set of M buck converters with the mentioned characteristic are stacked in parallel, the small-signal equivalent circuit can be represented as in Fig. 3.3. In this model, the output voltage dynamics for each converter are given by the capacitor voltage equation:

$$\frac{d\hat{v}_{o,m}}{dt} = \frac{1}{C_m}\left(\hat{i}_{L,m} + \frac{\hat{v}_{o,m} - \hat{v}_{cpl}}{r}\right). \tag{3.2}$$

The subscript m means that the variable belongs to the m-th converter, and the hat symbol "∧" indicates that the small-signal is being considered. The resistances of the lines that connect the capacitors and the CPL are named as r, they are considered equal for the sake of simplicity. Since the inductor current $i_{L,m}$ is set by the voltage PI compensator and the droop law (3.1), as observed in Fig. 3.3, its dynamics are defined by:

$$\hat{i}_{L,m} = K_{P,m} \cdot (\hat{V}_{sp} - \hat{v}_{o,m} - \hat{i}_{L,m} \cdot R_{d,m}) + K_{I,m} \int (\hat{V}_{sp} - \hat{v}_{o,m} - \hat{i}_{L,m} \cdot R_{d,m}) dt, \tag{3.3}$$

where K_p and K_I are the compensator's proportional and integral gains. In this case, the droop law is implemented by using the inductor current $i_{L,m}$ instead of the actual output current $i_{o,m}$. Since $i_{L,m}$ is equal to $i_{o,m}$ in steady-state this substitution still guarantees balanced current sharing and is a common practice in the literature. The CPL voltage, v_{cpl} in (3.2) is:

$$\hat{v}_{cpl} = \frac{R_{cpl}}{r + M \cdot R_{cpl}} \left(\sum_{m}^{M} v_{o,m} - \hat{I}_o \right), \tag{3.4}$$

where I_o is the output current operating point.

In order to analyze the stability using the small-signal equations, the system equations can be expressed in the form $\dot{\mathbf{x}} = \mathbf{A}\mathbf{x} + \mathbf{B}\mathbf{u}$. Then, the system's stability can be analyzed from the eigenvalues of $\mathbf{A}$. First, the following change of variable is done.

$$\frac{d\hat{w}_m}{dt} = \hat{V}_{sp} - \hat{v}_{o,m} - \hat{i}_{L,m} \cdot R_{d,m} \tag{3.5}$$

Now, equations (3.2) and (3.5) can be written using the state variables and system inputs only. In addition, if we do $\mathbf{u} = 0$ then:

$$\begin{bmatrix} \dot{\mathbf{w}} \\ \dot{\mathbf{v}} \end{bmatrix} = \mathbf{A} \cdot \begin{bmatrix} \mathbf{w} \\ \mathbf{v} \end{bmatrix}, \tag{3.6}$$

where $\mathbf{w} = [\hat{w}_1 \hat{w}_2 \cdots \hat{w}_m \cdots \hat{w}_M]^T$ and $\mathbf{v} = [\hat{v}_1 \hat{v}_2 \cdots \hat{v}_m \cdots \hat{v}_M]^T$. The matrix $\mathbf{A}$ and its entries are specified in equations (3.7)-(3.12) for the case of 3 parallel converters, and can be easily generalized to M converters.

$$\mathbf{A} = \begin{bmatrix} 0 & 0 & 0 & a_1 & b_1 & b_1 \\ 0 & 0 & 0 & b_2 & a_2 & b_2 \\ 0 & 0 & 0 & b_3 & b_3 & a_3 \\ e_1 & 0 & 0 & c_1 & d_1 & d_1 \\ 0 & e_2 & 0 & d_2 & c_2 & c_2 \\ 0 & 0 & e_3 & d_3 & d_3 & c_3 \end{bmatrix} \tag{3.7}$$

$$a_m = \frac{R_{d,m}}{r} \left(\frac{R_{\mathrm{cpl}}}{(r + 3\,R_{\mathrm{cpl}})} - 1 \right) - 1 \tag{3.8}$$

$$b_m = \frac{R_{\mathrm{cpl}}\,R_{d,m}}{r\,\left(r + 3\,R_{\mathrm{cpl}}\right)} \tag{3.9}$$

$$c_m = \frac{a_m\,K_{P,m}}{C_m} - \frac{(r + 2\,R_{\mathrm{cpl}})}{C_m\,r\,\left(r + 3\,R_{\mathrm{cpl}}\right)} \tag{3.10}$$

$$d_m = \frac{R_{\mathrm{cpl}}\,\left(K_{P,m}\,R_{d,m} + 1\right)}{C_m\,r\,\left(r + 3\,R_{\mathrm{cpl}}\right)} \tag{3.11}$$

$$e_m = \frac{K_{\mathrm{I},m}}{C_m} \tag{3.12}$$

Now, the matrix $\mathbf{A}$ is obtained for three parallel buck converters of different power rate. The variables and parameters of the system are normalized with respect to the base reference values of the middle power converter 2, and are summarized in Table 3.1. The eigenvalues of matrix $\mathbf{A}$ can be plotted in the complex plane in order to study the impact of a single fast controller on the stability of the system. The root locus analysis is done sweeping two different parameters: the gain of converter 2 ($K_{P,2}$), and the CPL power (P_{cpl}), which translates in a change of R_{cpl}.

The dominant poles of $\mathbf{A}$ when $K_{p,2}$ and $K_{I,2}$, are varied are observed in Fig. 3.4(a). From the figure, the effect that the increase in bandwidth of single converter has on the stability of the system can be analyzed. It is observed that two of its poles, originally located in the unstable region, become stable when the middle power converter's bandwidth is sufficiently large. The root locus when the $K_{P,2}$ is equal to $K_{P0,2}$, 3 $K_{P0,2}$, 10 $K_{P0,2}$, and 50 $K_{P0,2}$ are marked, where $K_{P0,2}$ corresponds to a compensator that is tuned for $f_{swn} \approx 80$ as indicated in Table 3.1. Figure 3.4(b) shows the voltage closed-loop magnitude Bode plots of converter

Table 3.1: Root Locus Analysis Normalized Parameters

Parameter	Formula	Conv. 1	Conv. 2	Conv. 3
$P_{n,X}$	$P_{ref,X}/P_{ref,2} = 1/Z_{0n,X}$	3/2	1	1/2
$Z_{0n,X}$	$Z_{0,X}/Z_{0,2}$	2/3	1	2
$F_{0n,X}$	$F_{0,X}/F_{0,2}$	0.8	1	1.2
$V_{ccn,X}$	-	1	1	1
$L_{n,X}$	$\frac{1}{2\pi}\frac{Z_{0n,X}}{F_{0n,X}}$	$\frac{5}{12\pi}$	$\frac{1}{2\pi}$	$\frac{5}{6\pi}$
$C_{n,X}$	$\frac{1}{2\pi}\frac{1}{Z_{0n,X}F_{0n,X}}$	$\frac{1}{2\pi}$	$\frac{15}{16\pi}$	$\frac{5}{24\pi}$
$r_{n,X}$	$r_n/Z_{0,2}$	0.01	0.01	0.01
$R_{dn,X}$	$0.4 \cdot Z_{0n,X}$	0.27	0.4	0.8
$f_{swn,X}$	$80 \cdot F_{0n}$	64	80	96
$K_{P0,X}$	-	1	1	1
$K_{I0,X}$	$0.01 \cdot f_{swn,X} \cdot K_{P0,X}$	0.64	0.8	0.96

2 for the mentioned values of $K_{P,2}$. The plots depict that the increase in bandwidth should be followed by an increase in the switching frequency, which sometimes is not possible and it can bring other disadvantages. For this particular case, $K_{P,2}$ should be increased three times for the system to be marginally stable. The consequent increase in the bandwidth is of two times, what requires the f_{sw} to be increased proportionally.

In Fig. 3.5, the impact that a fast controller has on the maximum stable load the system can operate at is studied. It is observed that the increase of $K_{P,2}$ in 10 times expands the maximum CPL power P_{cpln} at which the system is stable from 0.43 p.u. to 0.7 p.u. Note that the normalization of the power value is done as detailed in the equation:

$$P_{cpln} = \frac{P_{cpl}}{P_{ref}} = \frac{v_{cpl}^2}{R_{cpl}} \cdot \frac{Z_o}{V_{eq}^2}, \tag{3.13}$$

where Z_o and V_{eq} are the characteristic impedance and the equivalent voltage obtained in (2.11). Then, P_{cpln} is obtained for the case $v_{cpln} = 0.8$, where V_{eq} is used as normalizing base.

Finally, according to the Bode plots in Fig. 3.4(b), an increase of 10 times in $K_{P,2}$ would require f_{sw} to be increased 6 times in order to keep the proper separation with the closed loop crossover frequency.

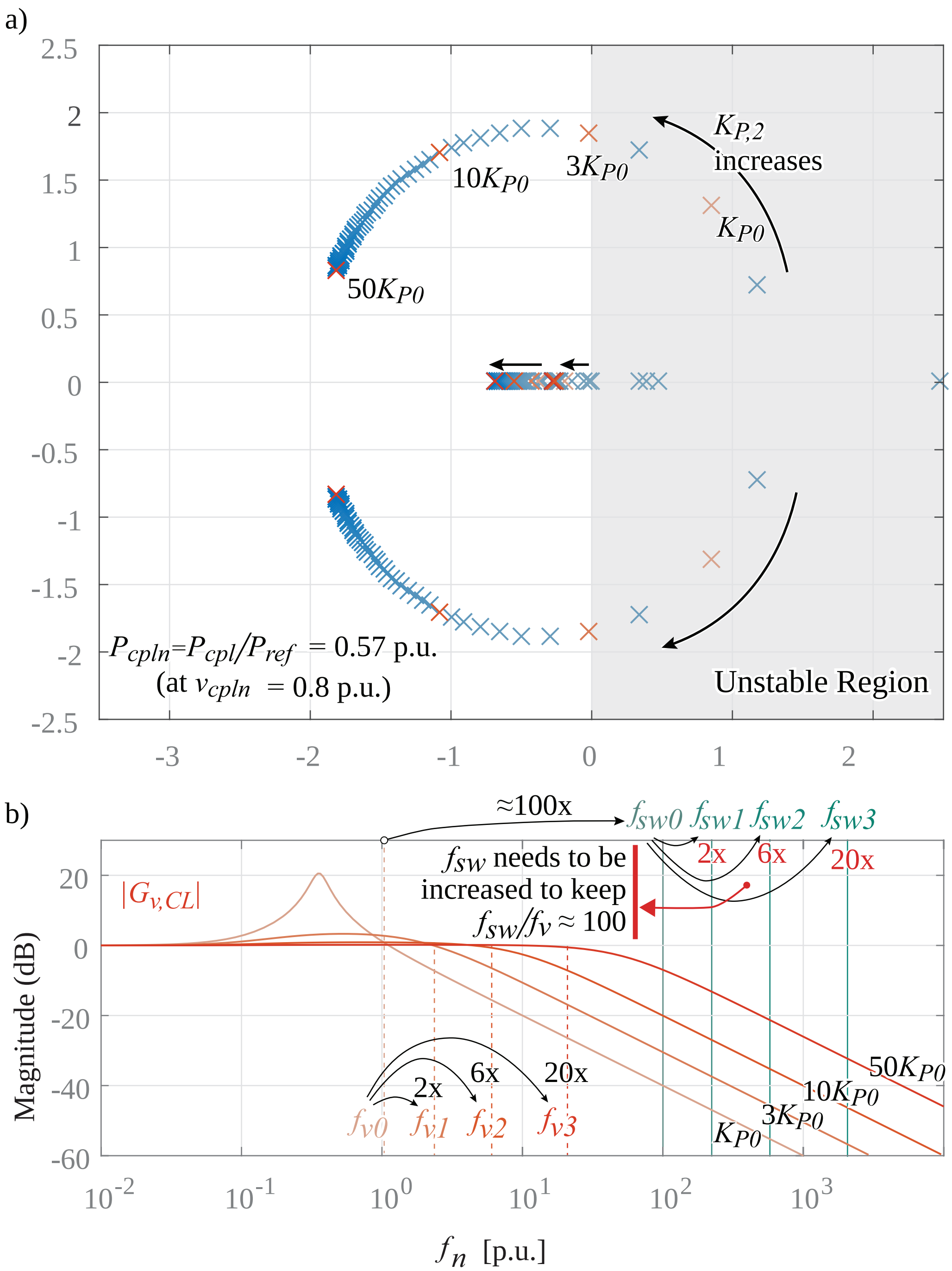

Figure 3.4: a) Dominant poles of a linearized model for M parallel buck converters controlled using nested dual PI compensators. The poles originally located on the RHP move to the LHP when the proportional gain of one of of the controllers is large enough. b) Bode plots that correspond to 4 different $K_{P,2}$ values of the parameter sweep. The increase of $K_{P,2}$ leads to increasing bandwidth that should be followed by a proportional increase of f_{swn}, which is often not desirable. The power value P_{cpln} is defined for a given R_{cpl} using (3.13).

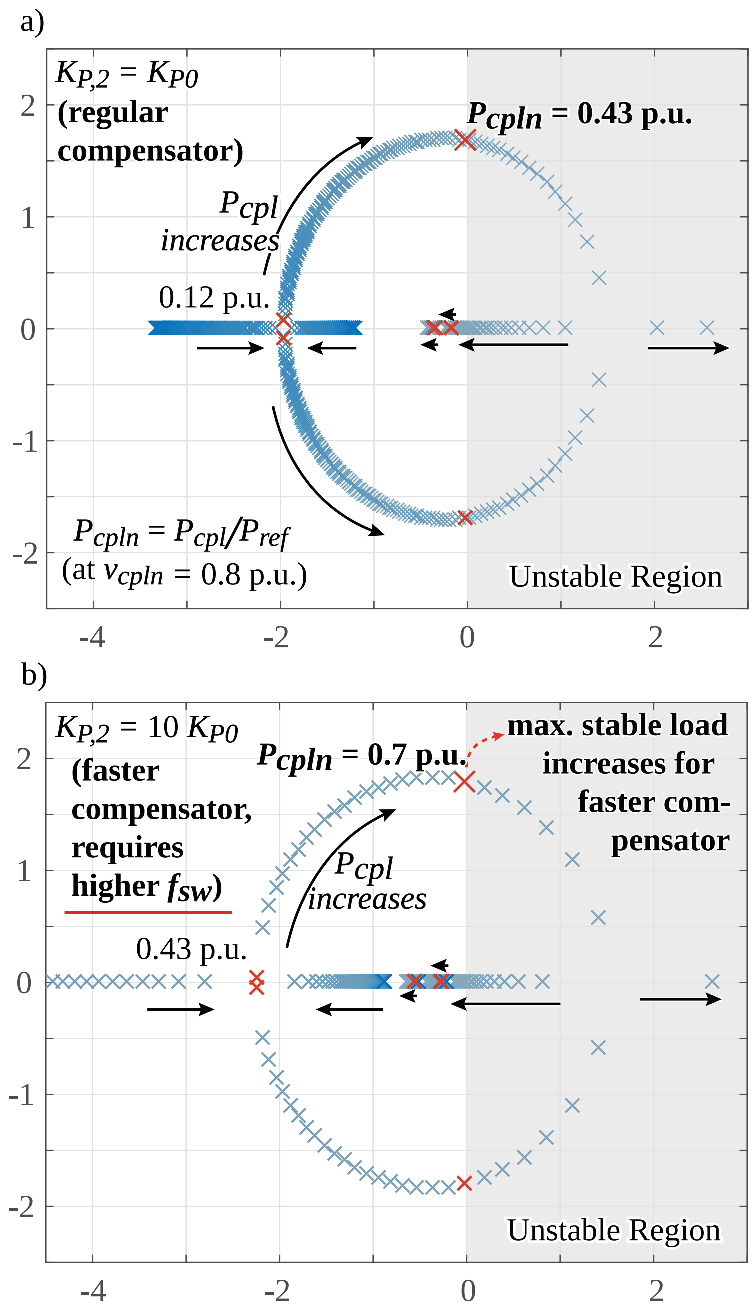

Figure 3.5: Dominant poles of a microgrid for load power sweep. The analysis is done for two different values of the proportional gain of the middle power converter ($K_{P,2}$). In b) $K_{P,2}$ is 10 times larger than in a), increasing the maximum CPL power at which the system is stable in 60% (0.7 p.u. vs. 0.43 p.u.). The power value P_{cpln} is defined for a given R_{cpl} using (3.13).

3.3 Tradeoff Between Droop Dynamics and CPL Transient Dynamics Robustness

The study of the system during CPL steps becomes necessary to understand its large signal behavior. In Fig. 3.5 the CPL step-up response for a model with three buck converters is shown when the bandwidth of one of the converters controllers is varied. The parameters are the same as the specified in Table 3.1. The results show that an increase in $K_{P,2}$ leads to a transitory imbalance in the current sharing that allows an improvement in the dc bus voltage dynamic regulation. The tradeoff that exists between dc bus voltage dynamic regulation and

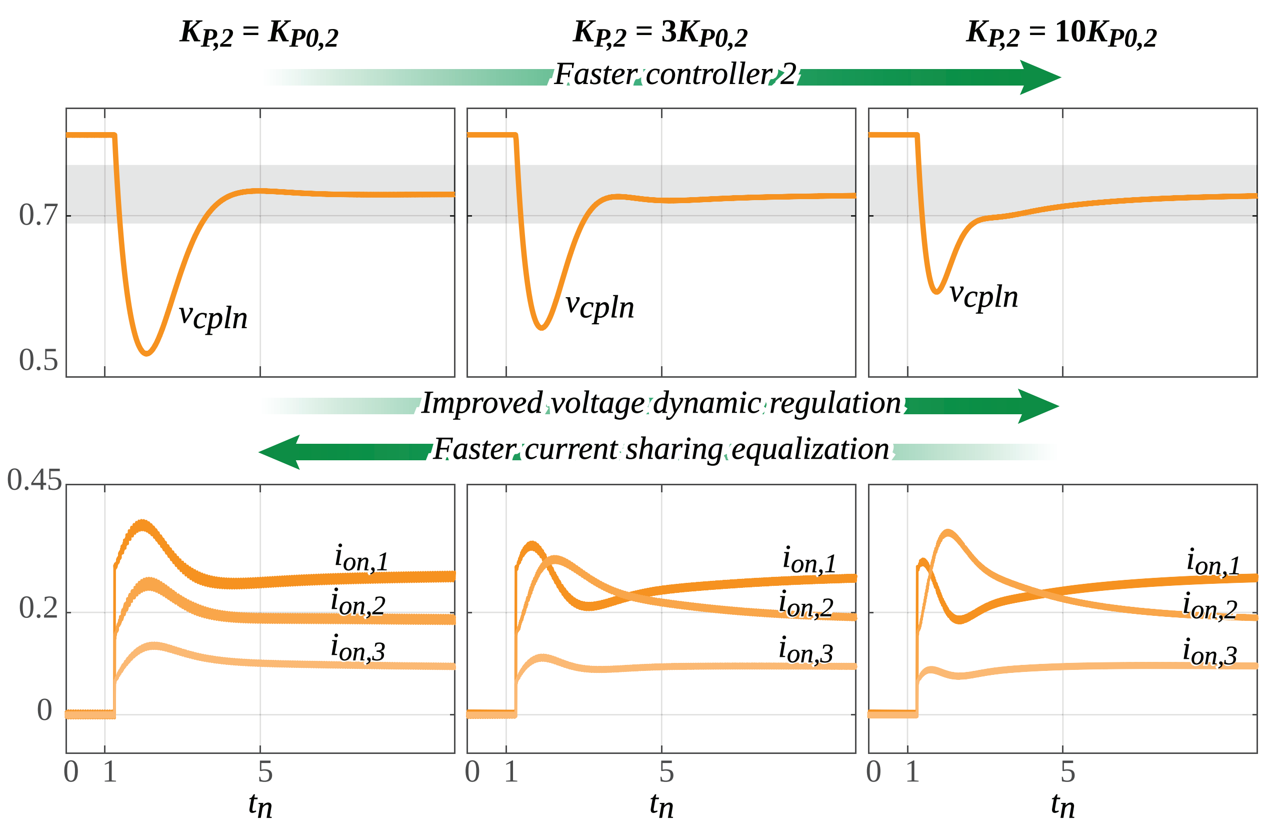

Figure 3.6: Tradeoff between droop dynamics and dc voltage dynamic regulation when a faster converter is introduced in the microgrid. A faster controller in one of the parallel converters of a microgrid improves the dc voltage regulation during CPL transients. The dissimilar speed in the converters leads to an transitory imbalance in the output currents right after the transient, what increases the currents settling time.

droop dynamics is depicted in the figure. Since the current of the faster controller grows faster during the transient, it can take a larger share of the load during the transient. When the voltage starts recovering the larger imbalance in the currents increases the settling time of currents and voltage. However, after the transient is over the current sharing is guaranteed. An unequal, but yet transitory, current sharing is necessary if the dynamics of the dc voltage are to be improved using a single faster converter.

3.4 Summary

This chapter introduced the concept of increasing the stability of a microgrid by using a faster controller in one of the source-end converters. The small signal stability of a linear model of a microgrid with a CPL was analyzed when using conventional dual PI compensators. For that purpose, the conventional dual PI compensator was first introduced and its bandwidth limitations were discussed. Then, the linear model of the microgrid was derived and its stability was analyzed from its root locus. The system dominant poles were obtained when varying the bandwidth of the middle power converter, and the CPL power. The analysis showed that having a faster controller in one of the converters of a microgrid increases the stability for a given CPL power and expands the maximum power at which the system can operate. Finally, the time domain large signal behavior of a microgrid was analyzed for the case of a CPL step-up, and the tradeoff between dc bus voltage dynamic regulation and droop dynamics was introduced and discussed.

Chapter 4

Circular Switching Surface Controller Under Droop Law

The use of a single faster controller in one of the source-end converters of a microgrid can lead to a general improvement of the stability and dc voltage dynamic regulation of the system. In chapter 3, it was noted that conventional dual-loop PI compensators have a limited dynamic response due to their bandwidth limitation. Their speed can only be improved at the cost of a larger switching frequency and the subsequent hardware specifications re-design. The use of other control schemes that can achieve fast response without increasing the steady state switching frequency is of interest to tackle this challenge. In particular, the Circular Switching Surface controller (CSS) features a very fast dynamic response. Since its control law is based on the knowledge of the possible trajectories that the converter describes in the state-plane, it is particularly effective during large-signal transients. Because of its faster dynamic response for a given hardware, the CSS controller will be chosen to replace one of the conventional dual PI controllers of the system. In this section, the CSS control law is derived including a modification of its target voltage that enables the converter to work under a droop control scenario. The behavior of the controller is first studied for the single converter case under a droop scheme and later compared with its performance in a microgrid.

4.1 Derivation of CSS for a Buck Converter Under Droop Control

Since the converter being controlled is operating within a dc microgrid, its target voltage (v_{on}^*) must follow a voltage droop law:

$$v_{on}^* = V_{spn} - R_{dn} \cdot i_{on}, \tag{4.1}$$

where, V_{spn} is the target voltage at no load, and R_d is the virtual droop resistance. Then, the target point of the CSS controller, given by ($v_{on}^*; i_{on}$), is not fixed but can be located at any point of the droop line. The CSS controller uses a geometrical approximation of the ON and OFF state-plane trajectories of the converter to base its control law. These trajectories can be obtained from the differential equations that describe the dynamics of the power converter. For the buck converter depicted in Fig. 2.1, the differential equations are given by (4.2) and (4.3). The time domain solutions are (4.4) and (4.5).

$$\frac{1}{2\pi}\frac{di_{Ln}}{dt_n} = uV_{ccn} - v_{on} \tag{4.2}$$

$$\frac{1}{2\pi}\frac{dv_{on}}{dt_n} = i_{Ln} - i_{on} \tag{4.3}$$

$$v_{on} = [v_{on}(0) - uV_{ccn}]\cos(2\pi t_n) + [i_{Ln}(0) - i_{on}]\sin(2\pi t_n) + uV_{ccn} \tag{4.4}$$

$$i_{Ln} = [i_{Ln}(0) - i_{on}]\cos(2\pi t_n) + [uv_{on}(0) - V_{ccn}]\sin(2\pi t_n) + i_{on} \tag{4.5}$$

Then, combining the expressions in (4.4) and (4.5), the time parameter t_n can be eliminated and the state-plane trajectories of the converter are obtained as in (4.6).

$$\lambda : (v_{on} - uV_{ccn})^2 + (i_{Ln} - i_{on})^2 - [v_{on}(0) - uV_{ccn}]^2 - [i_{Ln}(0) - i_{on}]^2 = 0 \tag{4.6}$$

The initial conditions $[v_{on}(0); i_{Ln}(0)]$ are given by any point in the state-plane that is contained in the converter's trajectory. Then, since the control law is based on the trajectories that passes through the operating point, (4.6) becomes:

$$\lambda : (v_{on} - uV_{ccn})^2 + (i_{Ln} - i_{on})^2 - (v^*_{on} - uV_{ccn})^2 = 0 \tag{4.7}$$

Equation (4.7) can be rewritten in the following form:

$$\lambda : (v_{on} - C_{von})^2 + (i_{Ln} - C_{iLn})^2 - R^2 = 0, \tag{4.8}$$

which is the equation of a circumference of radius R centered on $(C_{von}; C_{iLn})$. For small variations in i_{on}, the radius R can be approximated as constant. Then, when the control signal u is equal to 1, the converter ON trajectory can be described as a circular curve centered on $(V_{ccn}; i_{on})$. On the other hand, if the converter adopts the OFF structure, the converter trajectory describes a circumference centered on $(0; i_{on})$.

4.2 Control Law

The control law of the CSS controller is described using the two trajectories that result from (4.7) when v^*_{on} is defined by the droop law given in (4.1):

Case I: $(i_{iLn} > i_{on})$

if $(\sigma_1 > 0)$, *then* $u = 0$, *else* $u = 1$

Case II: $(i_{iLn} < i_{on})$

if $(\sigma_2 > 0)$, *then* $u = 1$, *else* $u = 0$

$$\textit{with} \begin{cases} \sigma_1 = v^2_{on} + (i_{Ln} - i_{on})^2 - (V_{spn} - R_{dn} \cdot i_{on})^2 \\ \sigma_2 = (v_{on} - V_{ccn})^2 + (i_{Ln} - i_{on})^2 - (V_{spn} - R_{dn} \cdot i_{on} - V_{ccn})^2. \end{cases}$$

As can be observed, the control law employes two circular surfaces, $\sigma_1 > 0$ and $\sigma_2 > 0$, to define the state of the switches. The switching surfaces are obtained from the ON and OFF circular trajectories that pass over the target operating point $(V_{spn} - R_{dn} \cdot i_{on}; i_{on})$. The two trajectories are obtained by replacing u with 1 or 0 in (4.7).

4.3 Control Law Operation: Single Converter and Microgrid Scenarios.

Figure 4.1 illustrates the start-up and step-up responses of a buck converter connected to a CPL that is being controlled by a CSS control law, which target voltage is defined by a droop law. It depicts the converter trajectories in both the state-plane and the time domain, and gives insight into the operation of the control law. During start-up, the converter's operating point corresponds to *Case I* of the control law. The compensator sets the converter in its ON structure until the operating point crosses the curve described by $\sigma_1 = 0$. At that moment, $\sigma_1 > 0$ and the control signal changes to $u = 0$. As i_{on} is constant during the start-up process, it can be observed that the converter's OFF trajectory matches the circular trajectory described by $\sigma_1 = 0$.

Once in ❸, the converter is subjected to a sudden power step-up. The rapid increase in current puts the converter under *Case II* and its control signal is set to 1 until it crosses $\sigma_1 = 0$. Since the CPL current varies as a function of its voltage (2.3), the radius of the ideal circle changes along the trajectory. The difference between the approximated circular trajectory ($\sigma_1 = 0$) and the trajectory (❹-❺) can be observed. Since the converter's operating point does not reach the target point with a single switching action, an extra switching action is required (❺). It is important to notice that, unlike in other applications, in this case, the target of the controller is not a point but the droop line.

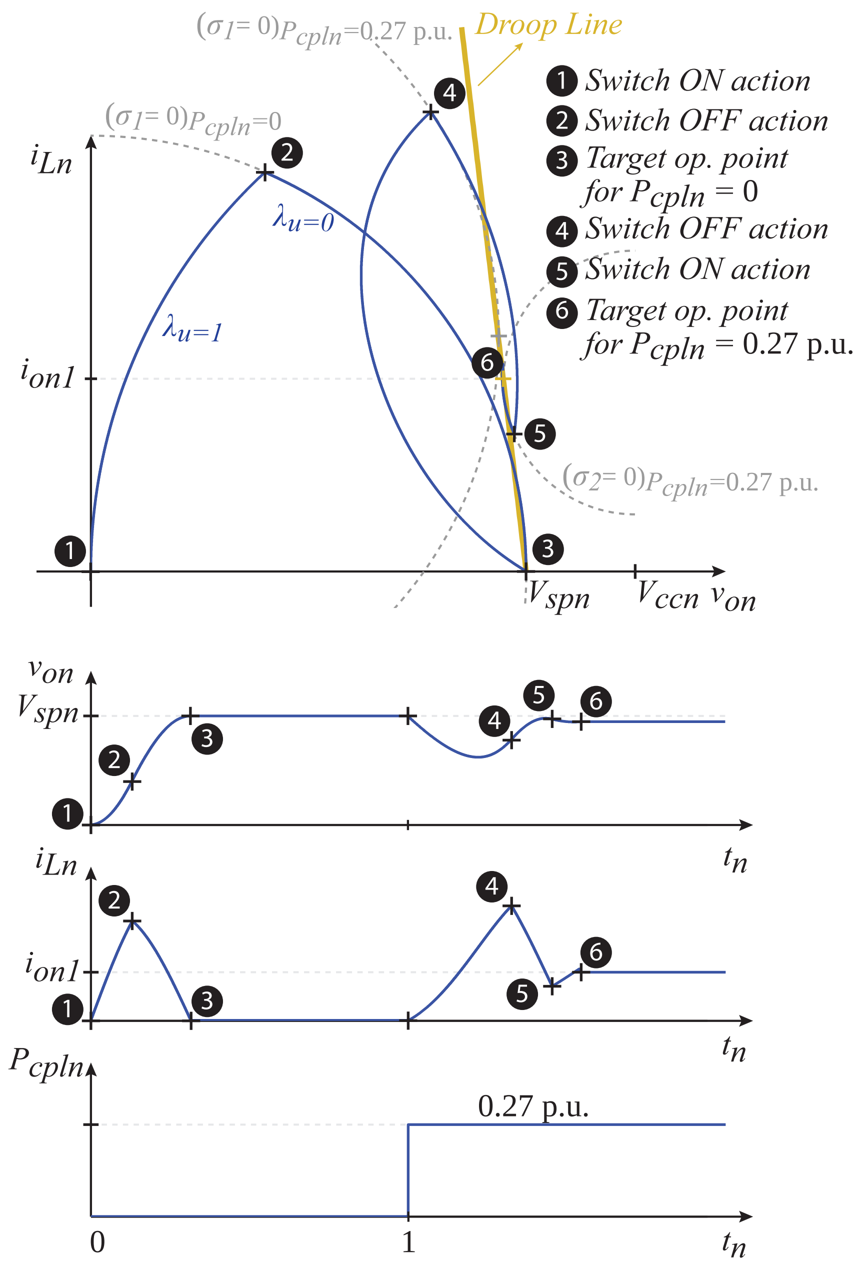

Figure 4.1: State-plane and time domain representations of start-up (❶-❸) and load step-up (❸-❻) transients of a buck converter with a CSS controller connected to a constant power load (CPL).

When the CSS controlled converter is in parallel with other slower converters in a micro-grid, its transient response can be affected by the interaction among converters. However, the circular approximation of the converter trajectories still describes the general behavior

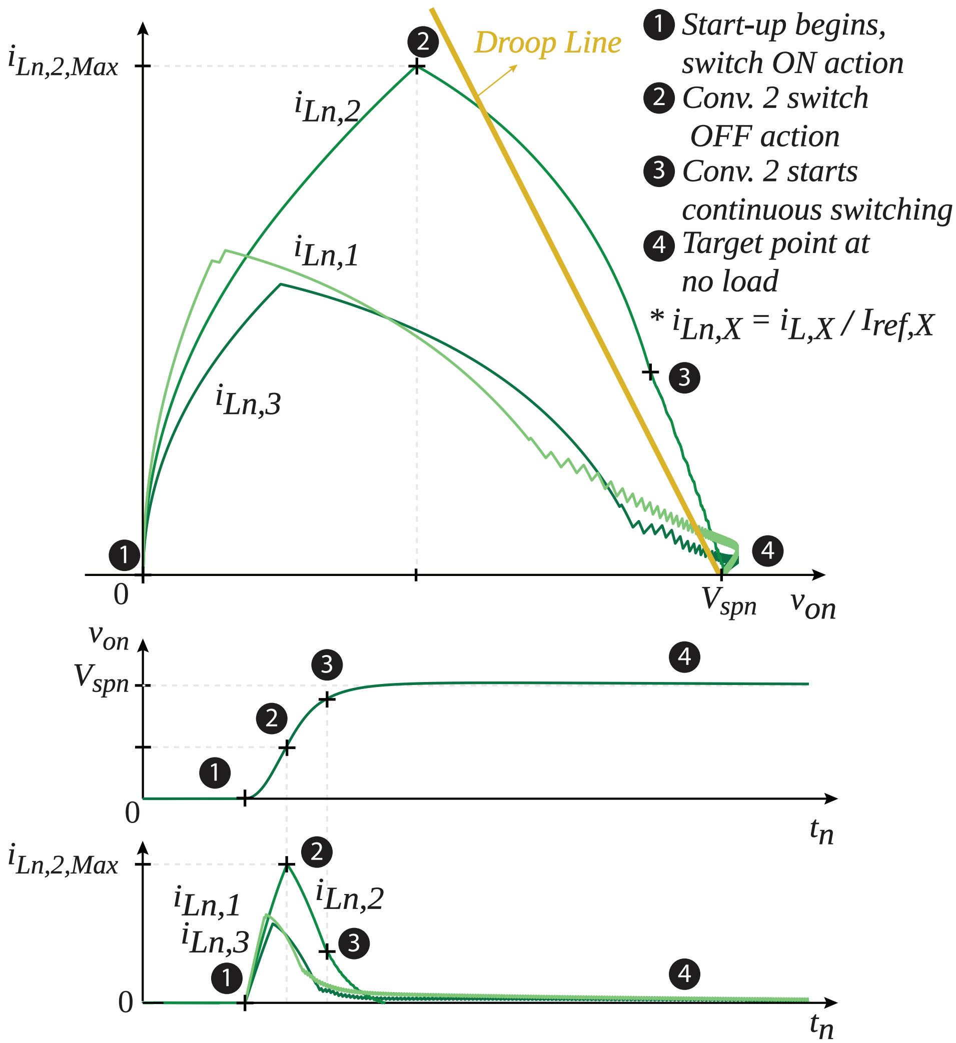

Figure 4.2: State-plane and time domain representations of synchronized start-up of three parallel converters connected to a constant power load (CPL). The middle power converter, with current $i_{Ln,2}$, uses a CSS controller.

of the converter in the state-plane domain. As seen for a single converter with a CPL, although the trajectory approximation is less accurate for large signal perturbations, it still describes the converter's general behavior and succeeds in bringing the operating point closer to the target value in very few switching actions. In an area close to the target point the trajectories estimation accuracy increases substantially guaranteeing convergence. A performance assessment of the use of a fast CSS controller in a microgrid is showed in Fig. 4.2 and

Fig. 4.3. The analysis shows how the use of a single CSS controller improves the performance for start-up and load step-up transient responses in a microgrid. The microgrid comprises three parallel converters with similar specifications as those in Table 3.1, with the exception that the middle power converter linear compensator is replaced with a CSS one. As done for the single converter case, the transients are shown in both the state-plane and the time domain. The inductor current of each converter ($i_{Ln,X}$) is normalized with respect to its own reference current ($I_{ref,X}$) in order to simplify the state-plane plots showing a single droop line instead of multiple ones.

The system is first analyzed for a synchronized start-up at no load. In Fig. 4.2, it is observed that the three converters switch ON right after the start-up begins (❶). However, converter 2 stays in the ON structure for a longer time, allowing $i_{Ln,2}$ to keep growing and the target voltage to be reached at a faster rate. In ❷ the control law command converter 2 to switch off, since it estimates that the OFF trajectory for the present operating conditions will lead the converter to the present target point. Since the operating point slides down in the droop line while the output current $i_{on,2}$ decreases, the target point changes continuously. This can be observed from ❸ to ❹ where the variation in the target point forces converter 2 to switch continuously until it reaches steady state ❹. Although this effect slows down the rate at which the steady-state target point could be reached, it is evident when the system is close to the target value and the transient is almost solved.

On the other hand, Fig. 4.3 shows the system's transient response for a CPL step-up. The state plane representation of the three converters trajectories shows how both controllers interact with the droop line. The plot shows that converter 2, with the CSS controller, hits the droop line within a few switching actions (❶). Its faster controller allows the inductor current to increase at a larger rate than that of the other two converters, and to reach the target value before. Once on the droop line, converter 2 moves on the straight line until it

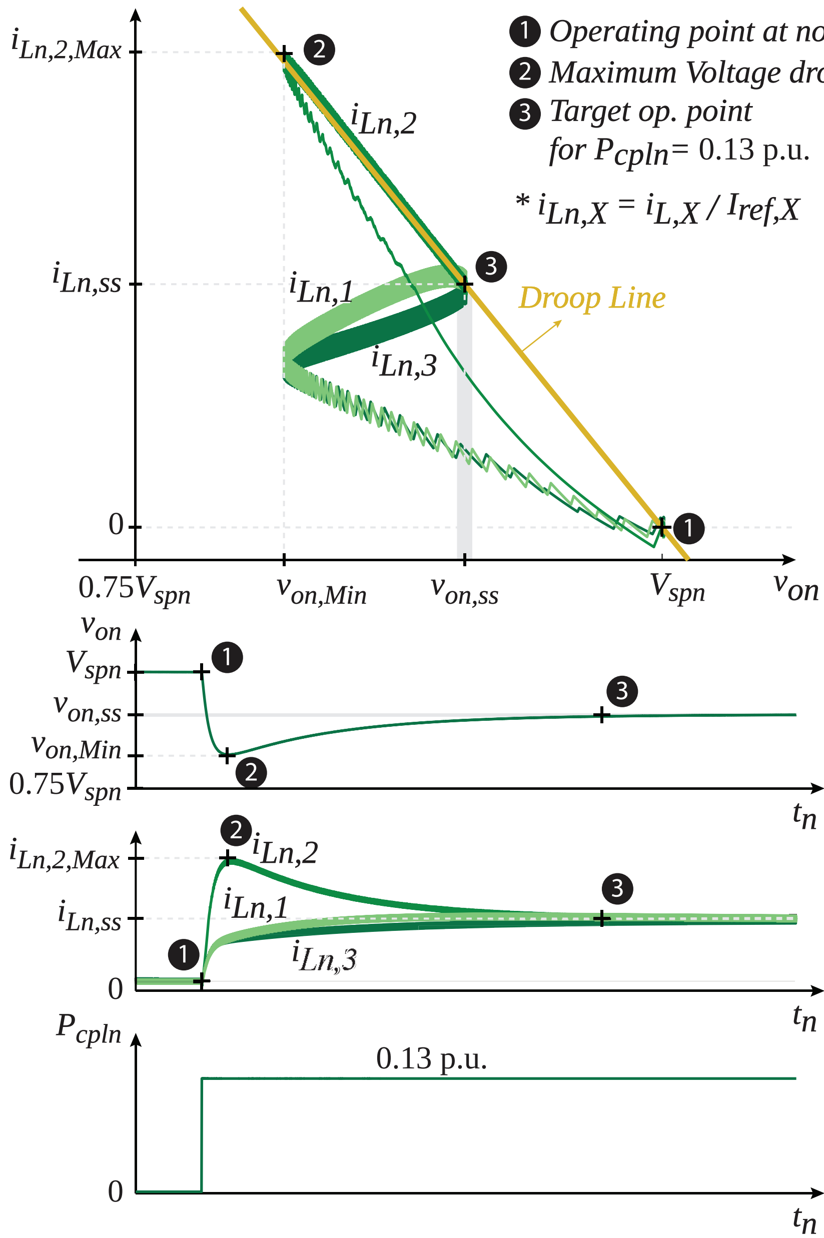

Figure 4.3: State-plane and time domain representations of a load step-up transient of three parallel converters connected to a constant power load (CPL). The middle power converter, with current $i_{Ln,2}$, uses a CSS controller.

reaches an operating point where the current is shared equally among the three converters (❸).

It is important to mention that although the CSS controller slides on the line as it may be expected for a sliding mode controller, its principle of operation is different and leads to dissimilar transient responses from initial to hitting point (❶-❷). Moreover, if the droop line is used as a sliding line, its slope does not guarantee that the converter will enter the region of existence right after the hitting point, which can lead to oscillations before the converter starts sliding. Then, if a sliding mode controller is implemented, its sliding line slope should be chosen adequately and will generally differ from that of the droop line.

4.4 Summary

In this chapter, the Circular Switching Surface controller (CSS) was introduced for its operation under a current sharing scenario. The control law bases its operation in a circular approximation of the converter trajectories in the state plane and includes a conventional droop law to enable its use for a converter in a microgrid. The operation of the CSS controller with embedded droop was first assessed for a single converter with a CPL. This simple scenario allowed to present the control operation for a simple case.

Later, the CSS control operation for a converter in parallel with other two converters, ruled with linear compensators, was assessed for start-up and CPL step-up transients. The inspection of the system transient responses revealed that the proposed control law allows the converter's current to increase at a faster rate during the transient, increasing the rate at which the target operating point is reached.

Chapter 5

Simulations and Parametric Analysis

While converters that are controlled using a CSS strategy, work very close to their physical limit, those that use conventional linear controllers, usually PI dual-loop, are tuned for a bandwidth several times lower than the plant's. Consequently, the substitution of linear controllers with CSS controllers within microgrids is expected to improve the individual dynamic performance of the converters and the combined bandwidth of the whole microgrid. The level of improvement that results from using the proposed approach can be assessed by comparing the performance of the different system configurations when subjected to large signal transients.

In this chapter, a simulation model is created to compare the performance of the traditional approach, where all the converters are controlled using conventional PI dual-loop compensators, and the proposed approach, where one compensator is substituted with a CSS one. The performance improvement of the proposed approach is assessed in terms of voltage dynamic regulation, and system resilience for a microgrid. In order to expand the results to a larger range of conditions, a parameter analysis is done in the second section of the chapter.

5.1 Simulations

A microgrid comprising three different converters powering a CPL is controlled using two different approaches and simulated using MATLAB/Simulink+PLECS. The converters are buck topologies of different power ratings. In a traditional strategy (case B), converters are

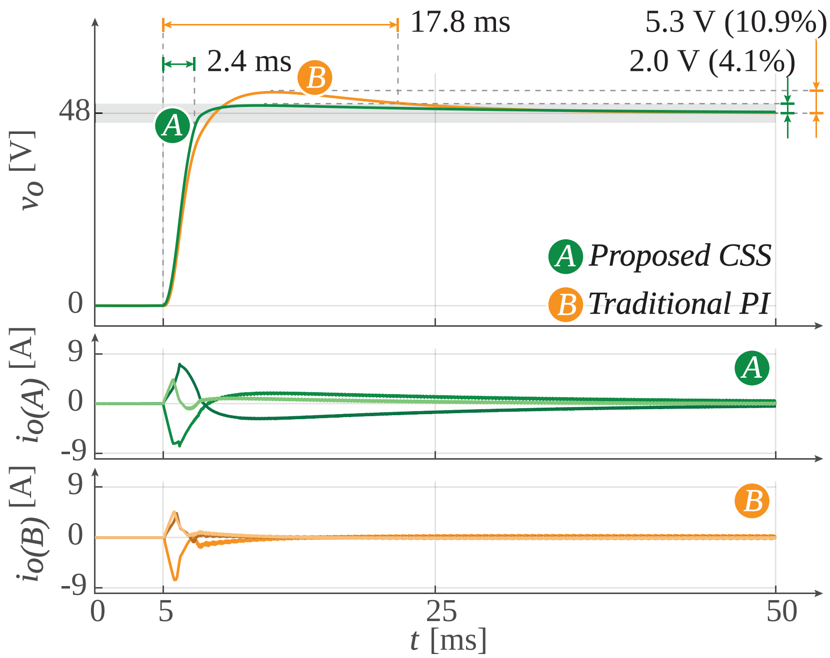

Figure 5.1: Simulation of a start-up transient for the proposed CSS (A) and traditional PI (B) approaches. Percentage of overshoot and settling time are measured for both strategies considering the 5% criterion. Case A is more than 7 times faster, and exhibits less than half of the overshoot.

controlled using traditional PI current-mode compensators. On the other hand, the proposed strategy (case A) involves replacing one of the controllers of the traditional approach system with a CSS one. Results of the simulations are presented for start-up, load step-up and load step-down transients in Fig. 5.1, 5.2 and 5.3 respectively. It is observed that the voltage dynamic regulation improves significantly for the strategy that replaces a linear controller with a CSS controller. It is noted how, during transients, the CSS-controlled converter supplies most of the current, avoiding major voltage drops in the dc bus. Moreover, Fig. 5.4 shows the simulation results of the two system configurations for different power steps. The proposed approach withstands higher power steps before becoming unstable, showing it can get closer to the theoretic critical power step specified in Fig. 2.2(b). for the given initial conditions.

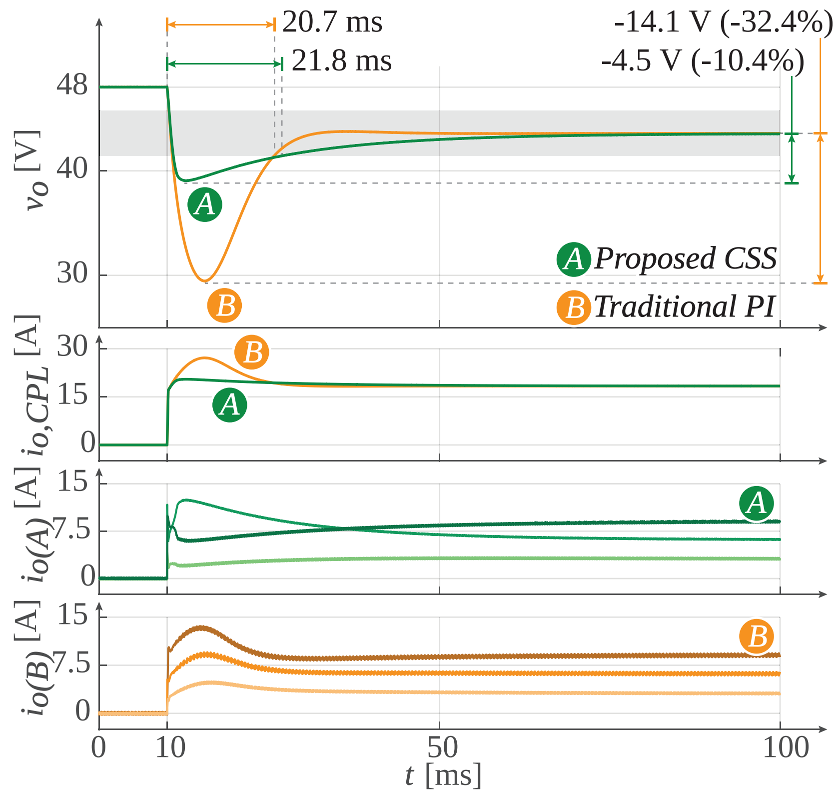

Figure 5.2: Simulation of a load step-up transient for the proposed (A) and traditional (B) approaches. Percentage of overshoot and recovery time are measured considering the 5% criterion. Cases A and B do not present a considerable difference in their recovery time. However, case B shows a dramatic voltage drop that is 3 times larger than case (A).

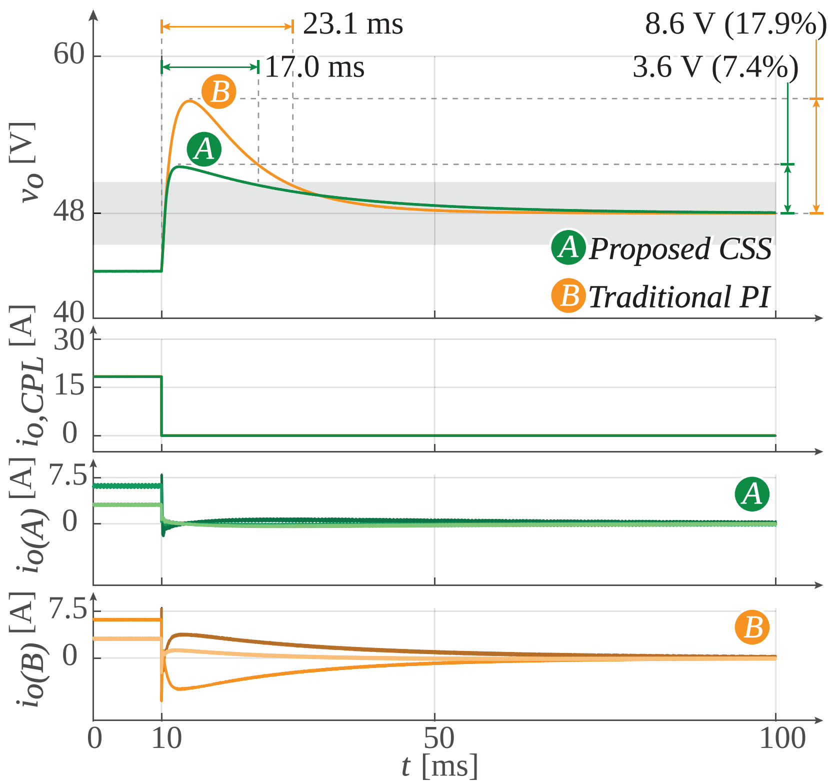

Figure 5.3: Simulation of a load step-down transient for the proposed CSS (A) and traditional PI (B) approaches. Case A presents much smaller overshoot when compared to 17.9% of case B, and a decrease in the transient recovery time.

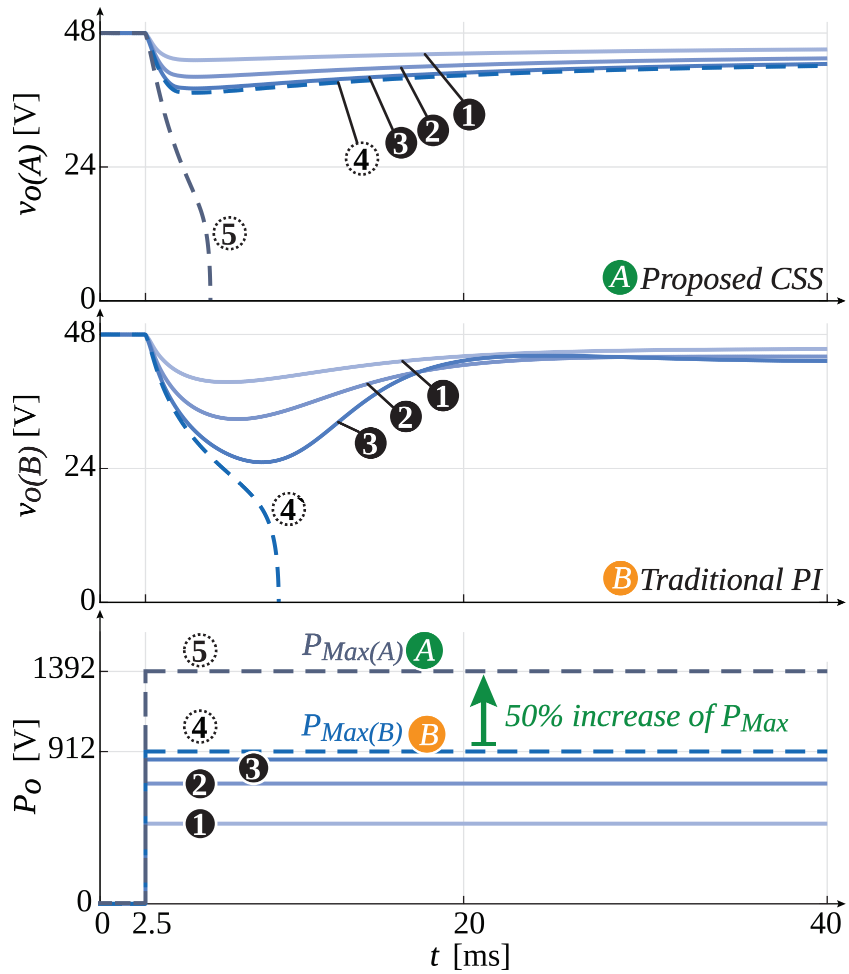

Figure 5.4: Microgrid dc bus voltage response for different power step-up values. Simulation results for the proposed CSS (A) and the traditional PI (B) approaches. Simulations for the proposed approach show that the microgrid can withstand larger power steps (up to 50% larger) while remaining stable.

5.2 Parametric Analysis

In order to test the validity of the proposed approach on a wider range of system conditions, a parametric analysis is performed. The study is done with a system of three buck converters in order to assess the impact that both the bandwidth of the linear controllers and the use of CSS compensators have on the critical power step of the system and the voltage drop during transients. The study is performed in the normalized domain as it was done in previous chapters, where converter 2 base quantities were used as normalizing values. The microgrid of three parallel converters shares most of its parameters with the approximated model analyzed in section 3.2. In this section, Table 5.1 is expanded to Table 3.1 to include those parameters that were not used in the linear model approximation. This time, a more comprehensive model of a microgrid of three parallel buck converters with normalized power 1, 2/3 and 1/3 p.u. is analyzed for different system configurations. The parametric sweep requires

Table 5.1: Simulations Parameters

Parameter	Formula	Conv. 1	Conv. 2	Conv. 3
$P_{n,X}$	$P_{ref,X}/P_{ref,2} = 1/Z_{0n,X}$	3/2	1	1/2
$Z_{0n,X}$	$Z_{0,X}/Z_{0,2}$	2/3	1	2
$F_{0n,X}$	$F_{0,X}/F_{0,2}$	0.8	1	1.2
$V_{ccn,X}$	-	1	1	1
$L_{n,X}$	$\frac{1}{2\pi}\frac{Z_{0n,X}}{F_{0n,X}}$	$\frac{5}{12\pi}$	$\frac{1}{2\pi}$	$\frac{5}{6\pi}$
$C_{n,X}$	$\frac{1}{2\pi}\frac{1}{Z_{0n,X}F_{0n,X}}$	$\frac{1}{2\pi}$	$\frac{15}{16\pi}$	$\frac{5}{24\pi}$
$R_{dn,X}$	$0.4 \cdot Z_{0n,X}$	0.27	0.4	0.8
$f_{swn0,X}$	$80 \cdot F_{0n}$	4	80	96
$Ki_{P0,X}$	-	10	10	10
$Ki_{I0,X}$	$0.7 \cdot f_{swn0,X} \cdot Ki_{P0,X}$	44.8	56	67.2
$Kv_{P0,X}$	-	1	1	1
$Kv_{I0,X}$	$0.01 \cdot f_{swn0,X} \cdot Kv_{P0,X}$	0.64	0.8	0.96

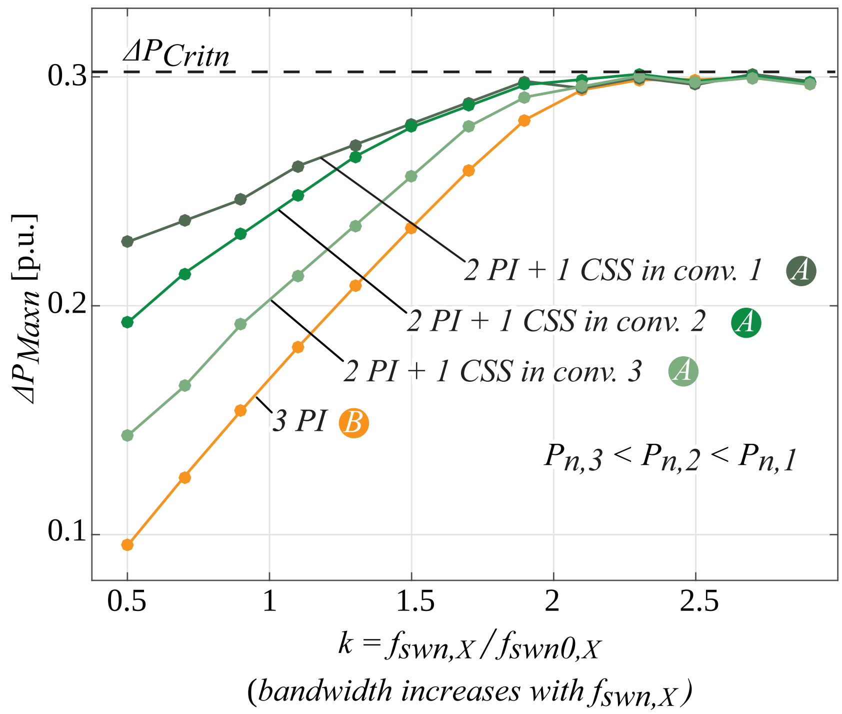

Figure 5.5: Maximum power step (CPL) vs. compensators' bandwidths for a microgrid comprising three converters, which are controlled using four different approaches. The bandwidth of each linear compensator is approximately proportional to the normalized switching frequency. For the proposed approach (A), the systems can withstand larger power steps at lower switching frequencies than it does for the traditional case (B). When the bandwidth of the linear compensators is increased, ΔP_{Maxn} for all the cases tends to the theoretical maximum ΔP_{Critn}. Moreover, the improvements in stability are larger when the relative power rate of the CSS-controlled converter is larger.

varying the bandwidth of the converters with linear compensators. The bandwidth is modified by multiplying the converter's nominal switching frequency $f_{swn0,X}$ and the compensators nominal gains $Ki_{P0,X}$, $Ki_{I0,X}$, $Kv_{P0,X}$, and $Kv_{I0,X}$ by a constant k. The nominal parameters are those that result from tuning the compensators with $f_{swn} \approx 80$.

Two different sets of simulations are performed. The analysis of the results of the first set of simulations is depicted in Fig. 5.5, and shows how the maximum stable power step increases when the bandwidth of the converters with linear compensators are expanded by doing k larger than 1. The influence of the use of CSS compensators on the maximum stable power

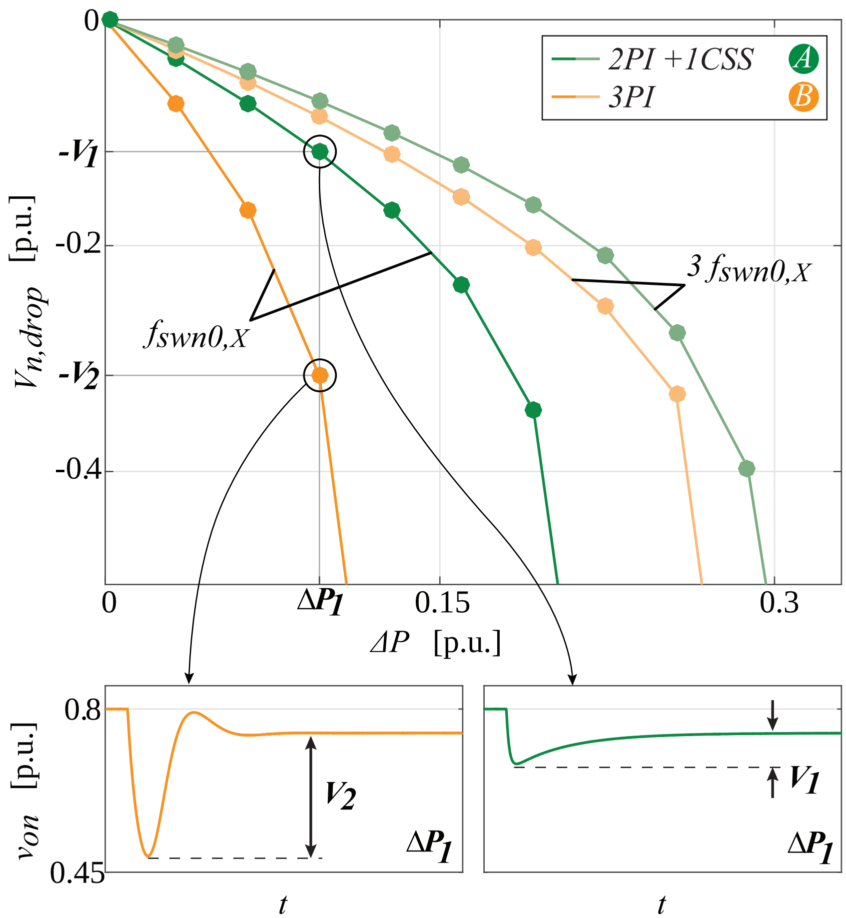

Figure 5.6: Voltage drop within a load step-up transient vs. power step for different compensators' bandwidths. The proposed case (A) shows a smaller voltage drops than does the traditional case (B). The difference increases when the switching frequency of the linear compensator is lower.

step ΔP_{Maxn} is assessed when comparing the results of the simulations across four system configurations. In the first setup, the three buck converters are controlled using only two nested PI loops (3PI), while in the other three cases, one of the converters' compensators is replaced with a CSS one (2PI+1CSS). For a given k it is observed that the 3PI setup presents lower ΔP_{Maxn} than do the 2PI+1CSS setups. Moreover, when the power rate of the CSS converter increases, the system maximum power step also increases. The analysis shows the capability of CSS-controlled converters to increase the stability margin of the system. When k increases so does the switching frequency and the linear compensators' bandwidth, and the behavior of each converter gets closer to its physical limit. In this case, when $f_{swn,X}$ double with respect to the nominal frequency $f_{swn0,X}$ ($k = 2$), the system ΔP_{Maxn} gets very close to the theoretical maximum ΔP_{Critn} (found in section 2.1). The results of this analysis show the system's large-signal stability improvement when the speed of the converters' controllers is increased, and are aligned with the analysis done in section 3.2 for small signal stability.

The analysis of the results of the second set of simulations is presented in Fig. 5.6. This figure shows the voltage drop of the dc bus during a load power step-up transient for different power step values. Both the proposed and traditional approaches are simulated for two different sets of switching frequencies, and the linear compensators' bandwidth is adjusted accordingly. It is observed that the 2PI+1CSS setup results in lower voltage drop for any power step. As was noticed in the first set of simulations, when the switching frequency is increased together with the PI compensators' bandwidth, both approaches present a similar behavior.

5.3 Summary

In this chapter, a model of a microgrid with three parallel converters was simulated for two main different approaches. The traditional approach (B) comprised converters controlled using conventional PI dual-loop compensators, while the proposed approach (A) replaced one of the compensators with a CSS faster controller. The results for approach A showed better dynamic regulation for start-up and CPL steps transients, and larger resilience under CPL step-up events. Moreover, a parametric analysis was done to expand the range of system conditions and include the effect of the bandwidth of the linear compensators for both approaches. Results showed that an increase in bandwidth in the linear controllers improves the overall system performance, but this happens at expense of a larger switching frequency. The proposed approach results present lower levels of voltage drop and better resilience during CPL step-ups transients for all the conditions analyzed. If compared with the proposed scenario, approach B would need to increase the switching frequency of their converters significantly, to achieve the same performance.

Chapter 6

Experimental Results

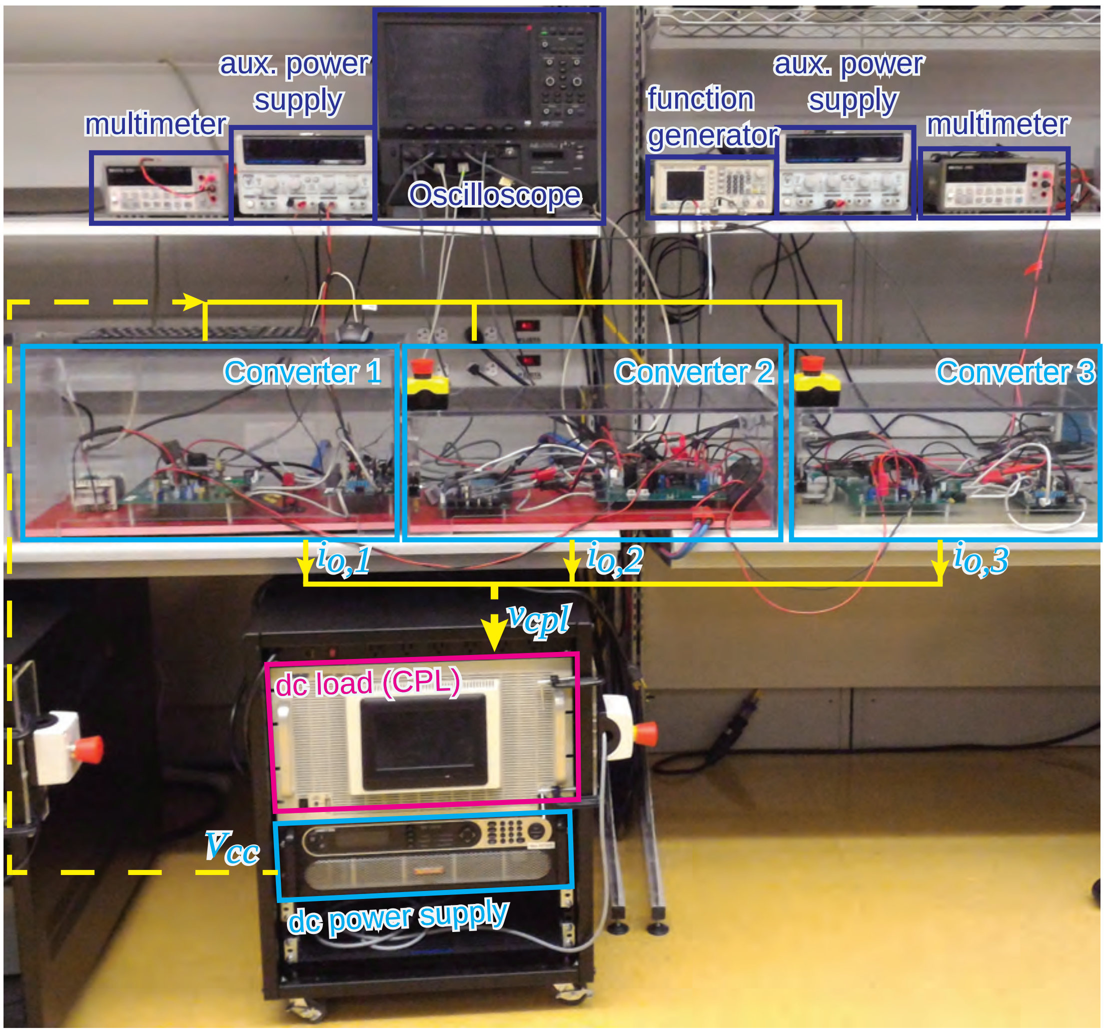

Figure 6.1: Photograph of the experimental setup

Table 6.1: Experimental Parameters

Parameter	Value Conv. 1	Value Conv. 2	Value Conv. 3
V_{cc}	60 V	60 V	60 V
V_{ref}	48 V	48 V	48 V
R_{droop}	0.48 Ω	1.8 Ω	3.6 Ω
L	1.9 mH	2.3 mH	4.0 mH
C	1200 μF	680 μF	330 μF
f_o	105 Hz	127 Hz	138 kHz
f_{sw}	8 kHz	10 kHz	12 kHz

The setup simulated in chapter 5, consisting of three parallel buck converters supplying a CPL, was implemented in an experimental platform, which photograph can be observed in Fig. 6.1, with the parameters detailed in Table 6.1.

The converters were synchronous buck prototypes working at a maximum power rate of 400 W each, and were controlled locally using a TI TMS320F28335 DSP. The circuit's load was an NHR 4760 dc electronic load configured in constant power mode and the dc power supply is an AMETEK Sorensen SGI 100/150. A function generator was used to synchronize the converters turn-on and turn-off in order to be able to capture the start-up transient. Experimental results of the system for start-up and load step-up and step-down transients are displayed in Figs. 6.2 to 6.4.

Fig. 6.2 b) shows a synchronized start-up of the linear-controlled converters when no load is present. The same transient is repeated when the compensator in converter 2 is replaced with a CSS controller. The results for the proposed approach are shown in Fig. 6.2 a), showing a 2.8 times decrease in the overshoot of the dc bus and a 6.7 times faster settling time compared with the results obtained using the traditional approach.

Figs. 6.3 shows the results for an 800 W CPL step-up. In this case, the dynamics of the droop control are responsible for the slow response and no significant difference can be appreciated between both settling times. However, a decrease of almost 3 times can be observed for the negative overshoot of the output voltage.

CPL step-down transients for both approaches are shown in Figs. 6.4. Once more, a reduction in the overshoot is observed when using the CSS approach (2.3 times). Moreover, the settling time is decreased from 18.4 ms to 12.4 ms.

Finally, Fig. 6.5 b) shows the response of the linear-controlled system crossing the limit of stability after a 900 W step-up is applied. On the other hand, when converter 2 employs a CSS control instead of the traditional current-mode control, the whole system can withstand a CPL step-up of at least 1080 W (20% higher), as shown in Fig. 6.5 a).

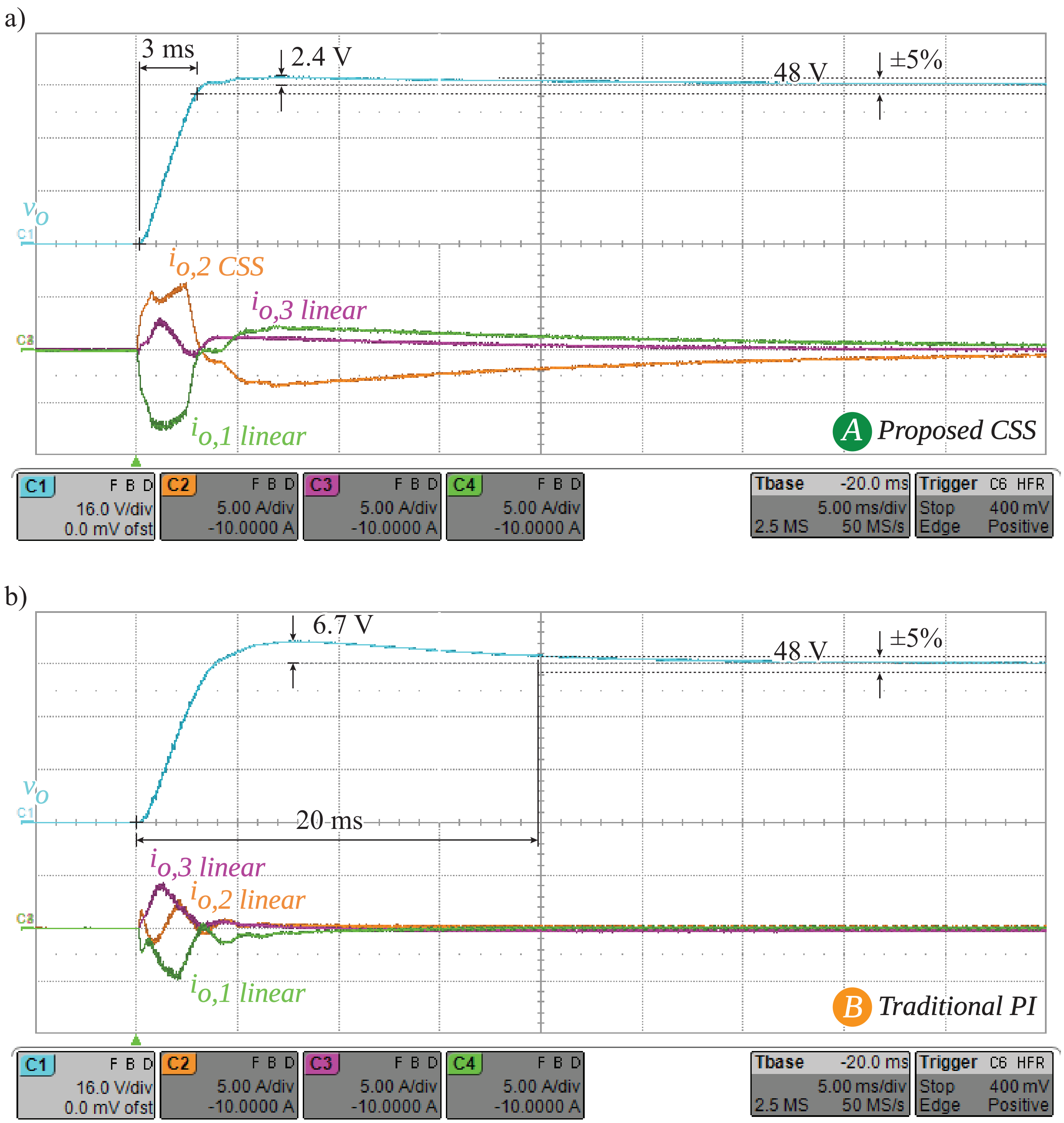

Figure 6.2: Experimental results of a start-up transient in a microgrid comprising three linear controlled converters. a) shows the proposed approach (A) when the controller of converter 2 is replaced with a CSS controller; and b) is the result for the traditional approach, where the three converters are controlled with linear PI controllers. (A) shows a smaller voltage overshoot (almost 3 times lower) and faster settling time (almost 7 times faster) than does (B).

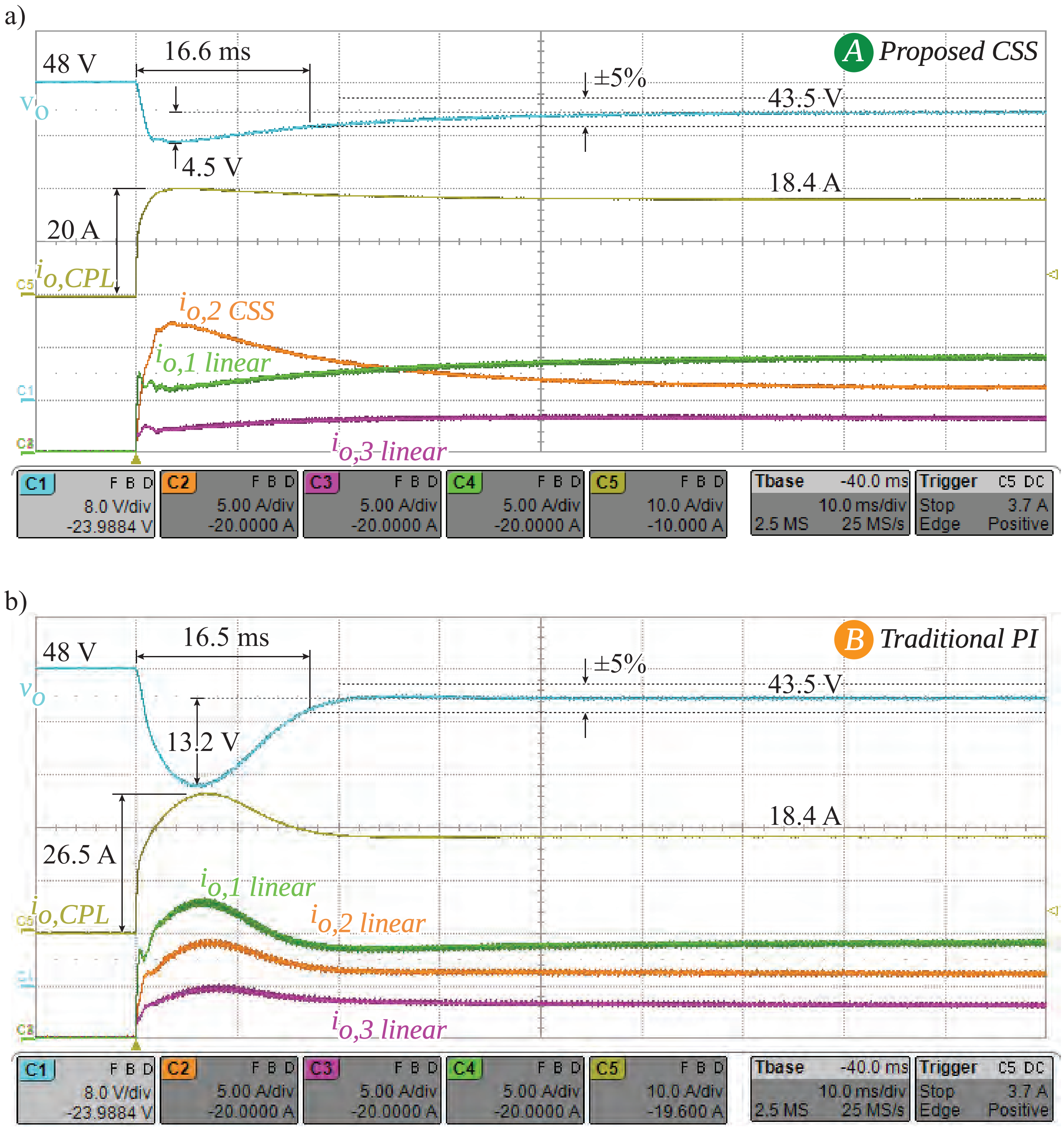

Figure 6.3: Experimental result of a 800 W CPL step-up transient. a) proposed approach (A), (compensator in converter 2 is replaced with a CSS controller); and b) traditional approach (B) for the traditional approach. The proposed approach (A) shows a smaller voltage drop (almost 3 times lower) than does the traditional approach (B).

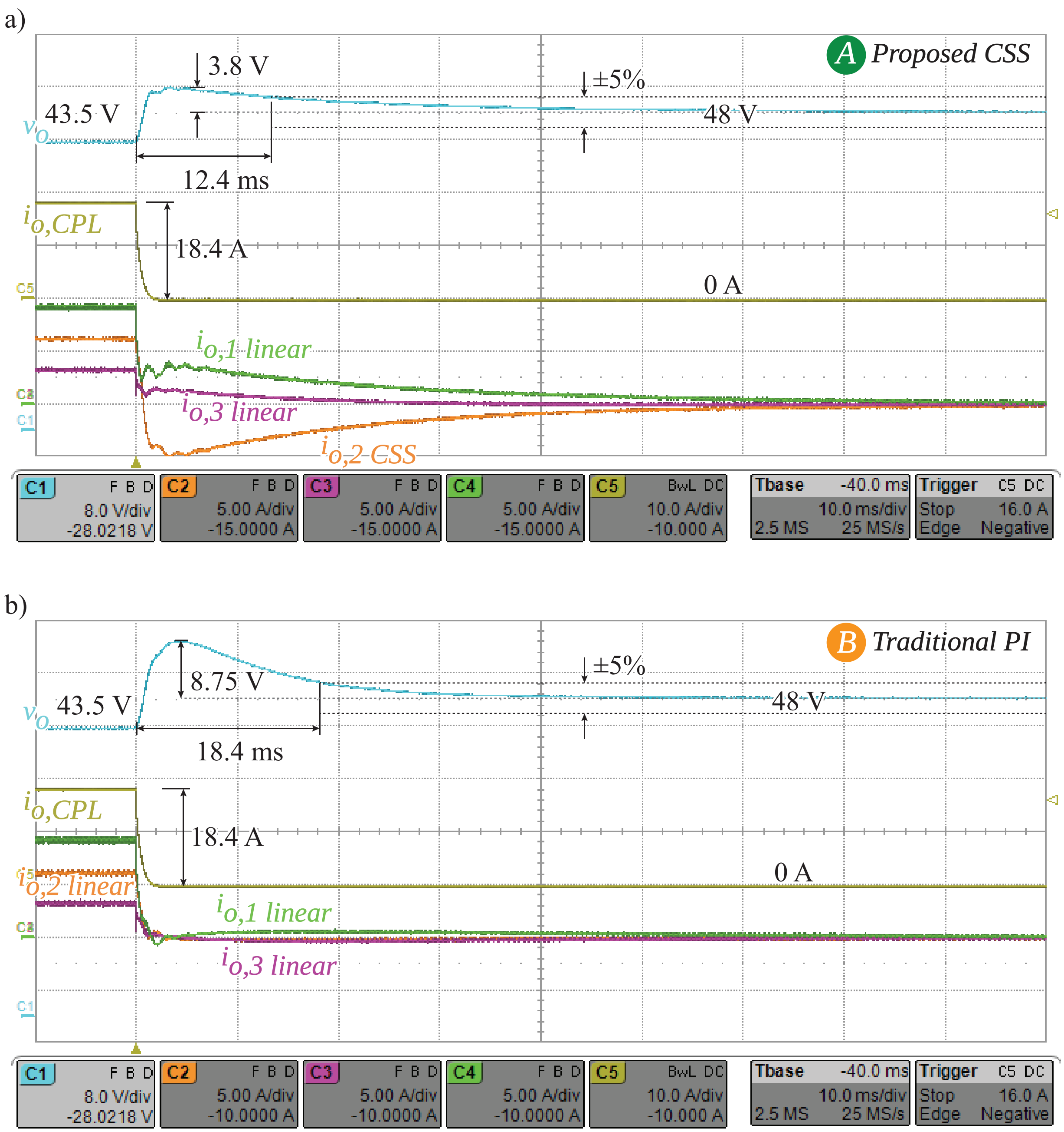

Figure 6.4: Experimental result of a 800 W CPL step-down transient for the traditional approach. a) proposed approach (A), (compensator in converter 2 is replaced with a CSS controller); and b) traditional approach (B) for the traditional approach. (A) has a smaller voltage overshoot (less than 2 times lower), and faster recovery time (30% improvement) than does (B).

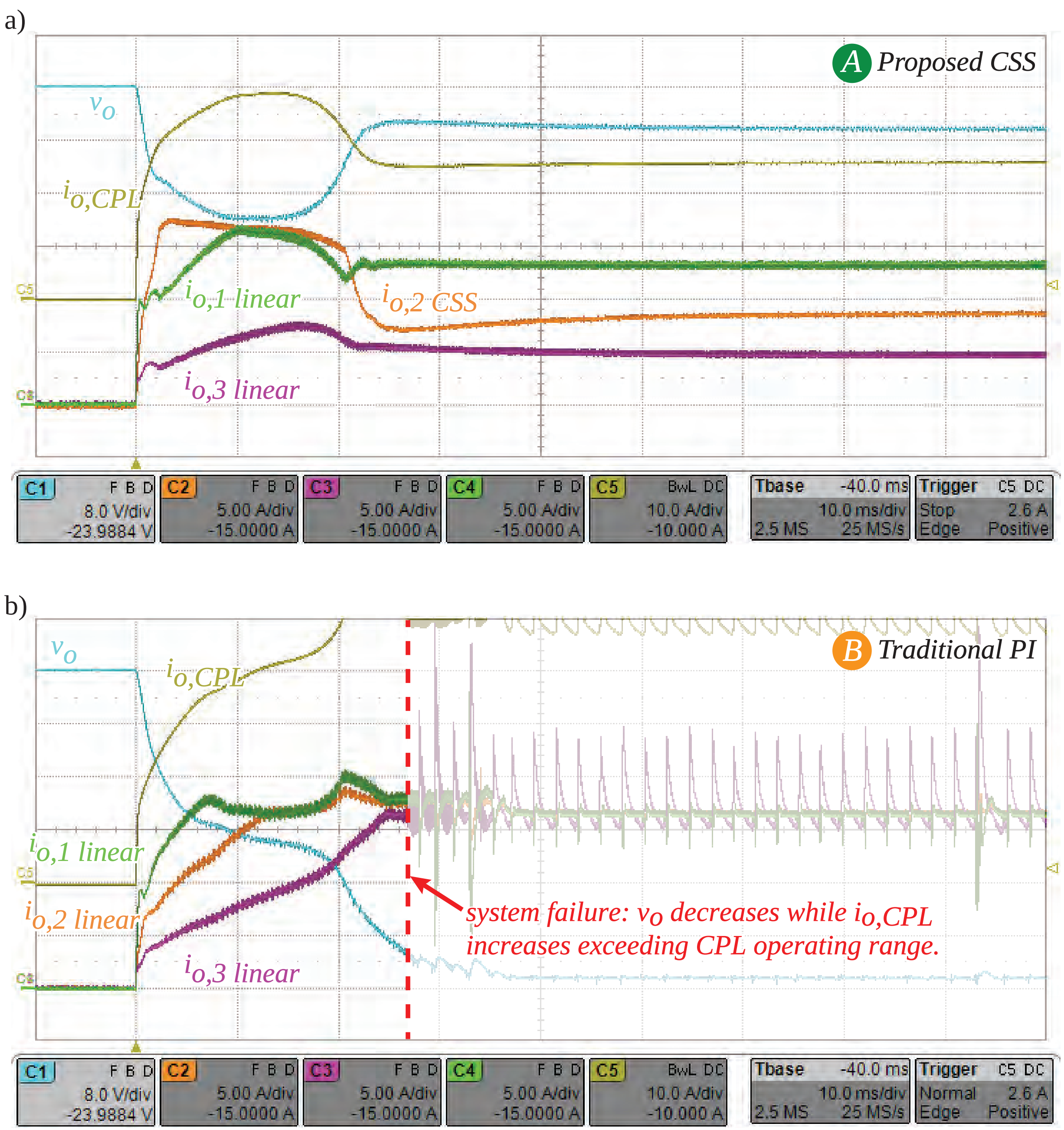

Figure 6.5: Experimental result showing maximum CPL step-up that the system can withstand for both approaches. a) proposed approach (A) for a 1080 W CPL step-up Experimental; b) traditional approach (B) for a 900 W CPL step-up. The use of a CSS controller in one of the converters in case (A) extends the maximum load step-up 20% if compared with the traditional approach (B).

Chapter 7

Conclusion

7.1 Summary

The presence of CPLs within microgrids leads to instability, observed in the dc bus as voltage oscillations, and as voltage drops after sudden load increments. This work introduced a CSS state-trajectory controller with an embedded droop law, to improve three critical aspects of the microgrid operation: 1) resiliency under large CPL's steps; 2) load transient voltage regulation; 3) voltage transient recovery time.

The negative effects of CPLs were studied in the state-plane domain and the theoretical maximum stable power-step (ΔP_{Crit}) was obtained, and generalized for a microgrid with parallel converters. ΔP_{Crit} can be employed as a benchmark to evaluate the performance of a given system and its source-end controllers.

The implications of having a faster controller in one of the source-end converters of the dc microgrid were analyzed using a linearized model, which was analytically derived. The model's root locus, obtained while varying the speed of one of the source-end controllers, showed that a single faster compensator can improve the small signal stability of the whole system. The tradeoff between current sharing dynamics and voltage regulation performance was noted, an unequal current sharing during the transient enables the faster converter to increase its load improving the transient performance. Moreover, the limitations of conventional nested dual-loop PI controllers were discussed, explaining the need for using a different control technique that does not require increased switching frequency in order to improve the system dynamic performance.

The CSS control law with embedded droop was derived for a buck converter, which is a structure frequently found in microgrids. Since the control law bases its operation on a circular approximation of the converter's state-plane trajectories, its performance assessment was explained and analyzed geometrically in the state-variables domain.

Then, a microgrid consisting of three buck converters connected in parallel to a CPL was simulated in MATLAB/Simulink+PLECS confirming the advantages of the proposed approach. A parametric analysis of a normalized version of the system was done to investigate the large signal behavior of the proposed approach. The results showed for a wide range of conditions that the proposed approach can withstand larger load step-ups with less voltage drop, and that switching frequency would need to be increased several times in order to obtain the same stability margins using PI current-mode compensators.

Finally, the system was implemented in an experimental platform comprised of three buck converters prototypes working at a maximum power of 400 W each. The converters were controlled using local DSPs and the system was loaded with an electronic load working in CPL mode. The experiments, run in the proposed setup for start-up, load step-up and load step-down transients, showed a reduction in overshoot of two to three times and a decrease in settling and recovery time for start-up and load step-down cases, as compared to the results obtained using the traditional setup. Moreover, the replacement of a single controller with a CSS control with embedded droop led to a 20% increase in the power level of the maximum CPL step that the system can withstand.

7.2 Future Work

The concept developed in this work provides an original contribution to the field of stabilization of dc microgrids under constant power loads. The work could be extended to different microgrid configurations with diverse converter topologies. In particular, its application in hybrid energy storage systems, where a single faster controller drives a super-capacitor bank, could be very effective.

Bibliography

[1] M. A. Bianchi, I. G. Zurbriggen, M. Ordonez, and M. Anun, "Dynamic performance improvement of dc microgrids during constant-power load transients," in *2016 IEEE 7th International Symposium on Power Electronics for Distributed Generation Systems (PEDG)*, June 2016, pp. 1–6.

[2] *REN21. 2017. Renewables 2017 Global Status Report*, 2017.

[3] R. H. Lasseter, "Microgrids," in *2002 IEEE Power Engineering Society Winter Meeting. Conference Proceedings (Cat. No.02CH37309)*, vol. 1, 2002, pp. 305–308 vol.1.

[4] R. Peña-Alzola, M. A. Bianchi, and M. Ordonez, "Control design of a pfc with harmonic mitigation function for small hybrid ac/dc buildings," *IEEE Transactions on Power Electronics*, vol. 31, no. 9, pp. 6607–6620, Sept 2016.

[5] X. Lu, K. Sun, J. M. Guerrero, J. C. Vasquez, L. Huang, and J. Wang, "Stability enhancement based on virtual impedance for dc microgrids with constant power loads," *IEEE Transactions on Smart Grid*, vol. 6, no. 6, pp. 2770–2783, Nov 2015.

[6] M. Su, Z. Liu, Y. Sun, H. Han, and X. Hou, "Stability analysis and stabilization methods of dc microgrid with multiple parallel-connected dc-dc converters loaded by cpls," *IEEE Transactions on Smart Grid*, vol. PP, no. 99, pp. 1–1, 2016.

[7] I. Kondratiev, E. Santi, and R. Dougal, "Nonlinear synergetic control for m parallel-connected dc-dc buck converters: Droop current sharing," in *2006 37th IEEE Power Electronics Specialists Conference*, June 2006, pp. 1–7.

[8] S. Anand and B. G. Fernandes, "Reduced-order model and stability analysis of low-voltage dc microgrid," *IEEE Transactions on Industrial Electronics*, vol. 60, no. 11, pp. 5040–5049, Nov 2013.

[9] J. M. Guerrero, J. C. Vasquez, J. Matas, L. G. de Vicuna, and M. Castilla, "Hierarchical control of droop-controlled ac and dc microgrids - a general approach toward standardization," *IEEE Transactions on Industrial Electronics*, vol. 58, no. 1, pp. 158–172, Jan 2011.

[10] A. Paquette and D. Divan, "Transient droop for improved transient load sharing in microgrids," in *Energy Conversion Congress and Exposition (ECCE), 2014 IEEE*, Sept 2014, pp. 84–91.

[11] Y. Tu, Z. Liu, J. Liu, T. Liu, and Z. Liu, "An additional stabilizer for mitigating the instability in dc/dc cascaded system with constant power loads," in *2017 IEEE 3rd International Future Energy Electronics Conference and ECCE Asia (IFEEC 2017 - ECCE Asia)*, June 2017, pp. 1982–1986.

[12] O. Pizniur, Z. Shan, and J. Jatskevich, "Ensuring dynamic stability of constant power loads in dc telecom power systems and data centers using active damping," in *2014 IEEE 36th International Telecommunications Energy Conference (INTELEC)*, Sept 2014, pp. 1–8.

[13] J. You, Z. P. Fan, Y. Hu, and M. J. Deng, "Virtual resistor based dbvc and active damping method for dc bus stabilization of cascaded power converters system," in *2017*

IEEE Transportation Electrification Conference and Expo, Asia-Pacific (ITEC Asia-Pacific), Aug 2017, pp. 1–6.

[14] X. Chang, Y. Li, X. Li, and X. Chen, "An active damping method based on a supercapacitor energy storage system to overcome the destabilizing effect of instantaneous constant power loads in dc microgrids," *IEEE Transactions on Energy Conversion*, vol. 32, no. 1, pp. 36–47, March 2017.

[15] M. Cespedes, L. Xing, and J. Sun, "Constant-power load system stabilization by passive damping," *IEEE Transactions on Power Electronics*, vol. 26, no. 7, pp. 1832–1836, July 2011.

[16] A. Kwasinski and C. N. Onwuchekwa, "Dynamic behavior and stabilization of dc microgrids with instantaneous constant-power loads," *IEEE Transactions on Power Electronics*, vol. 26, no. 3, pp. 822–834, March 2011.

[17] A. Riccobono and E. Santi, "Comprehensive review of stability criteria for dc distribution systems," in *2012 IEEE Energy Conversion Congress and Exposition (ECCE)*, Sept 2012, pp. 3917–3925.

[18] P. Magne, D. Marx, B. Nahid-Mobarakeh, and S. Pierfederici, "Large-signal stabilization of a dc-link supplying a constant power load using a virtual capacitor: Impact on the domain of attraction," *IEEE Transactions on Industry Applications*, vol. 48, no. 3, pp. 878–887, May 2012.

[19] P. Magne, B. Nahid-Mobarakeh, and S. Pierfederici, "Dynamic consideration of dc microgrids with constant power loads and active damping system -a design method for fault-tolerant stabilizing system," *IEEE Journal of Emerging and Selected Topics in Power Electronics*, vol. 2, no. 3, pp. 562–570, Sept 2014.

[20] X. Zhang, X. Ruan, and Q. C. Zhong, "Improving the stability of cascaded dc/dc converter systems via shaping the input impedance of the load converter with a parallel or series virtual impedance," *IEEE Transactions on Industrial Electronics*, vol. 62, no. 12, pp. 7499–7512, Dec 2015.

[21] F. Zhang and Y. Yan, "Start-up process and step response of a dc-dc converter loaded by constant power loads," *IEEE Transactions on Industrial Electronics*, vol. 58, no. 1, pp. 298–304, Jan 2011.

[22] Q. Shafiee, T. Dragievi, J. C. Vasquez, and J. M. Guerrero, "Hierarchical control for multiple dc-microgrids clusters," *IEEE Transactions on Energy Conversion*, vol. 29, no. 4, pp. 922–933, Dec 2014.

[23] D. Zammit, C. S. Staines, M. Apap, and A. Micallef, "Paralleling of buck converters for dc microgrid operation," in *2016 International Conference on Control, Decision and Information Technologies (CoDIT)*, April 2016, pp. 070–076.

[24] A. M. Rahimi and A. Emadi, "Active damping in dc/dc power electronic converters: A novel method to overcome the problems of constant power loads," *IEEE Transactions on Industrial Electronics*, vol. 56, no. 5, pp. 1428–1439, May 2009.

[25] M. Wu and D. D. C. Lu, "A novel stabilization method of lc input filter with constant power loads without load performance compromise in dc microgrids," *IEEE Transactions on Industrial Electronics*, vol. 62, no. 7, pp. 4552–4562, July 2015.

[26] M. K. Zadeh, R. Gavagsaz-Ghoachani, S. Pierfederici, B. Nahid-Mobarakeh, and M. Molinas, "Stability analysis and dynamic performance evaluation of a power electronics-based dc distribution system with active stabilizer," *IEEE Journal of Emerging and Selected Topics in Power Electronics*, vol. 4, no. 1, pp. 93–102, March 2016.

[27] P. Lin, P. Wang, J. Xiao, J. Wang, C. Jin, and Y. Tang, "An integral droop for transient power allocation and output impedance shaping of hybrid energy storage system in dc microgrid," *IEEE Transactions on Power Electronics*, vol. PP, no. 99, pp. 1–1, 2017.

[28] Q. Xu, X. Hu, P. Wang, J. Xiao, P. Tu, C. Wen, and M. Y. Lee, "A decentralized dynamic power sharing strategy for hybrid energy storage system in autonomous dc microgrid," *IEEE Transactions on Industrial Electronics*, vol. 64, no. 7, pp. 5930–5941, July 2017.

[29] S. K. Kollimalla, M. K. Mishra, A. Ukil, and H. B. Gooi, "Dc grid voltage regulation using new hess control strategy," *IEEE Transactions on Sustainable Energy*, vol. 8, no. 2, pp. 772–781, April 2017.

[30] C. H. Rivetta, A. Emadi, G. A. Williamson, R. Jayabalan, and B. Fahimi, "Analysis and control of a buck dc-dc converter operating with constant power load in sea and undersea vehicles," *IEEE Transactions on Industry Applications*, vol. 42, no. 2, pp. 559–572, March 2006.

[31] W. Du, J. Zhang, Y. Zhang, and Z. Qian, "Stability criterion for cascaded system with constant power load," *IEEE Transactions on Power Electronics*, vol. 28, no. 4, pp. 1843–1851, April 2013.

[32] I. G. Zurbriggen, M. Anun, and M. Ordonez, "Dual-loop geometric-based control of buck converters," in *2015 IEEE Applied Power Electronics Conference and Exposition (APEC)*, March 2015, pp. 392–396.

[33] I. G. Zurbriggen, M. Ordonez, and M. A. Bianchi, "Dual-loop geometric-based control of boost converters," in *2015 IEEE Energy Conversion Congress and Exposition (ECCE)*, Sept 2015, pp. 2072–2077.

[34] M. A. Bianchi, I. G. Zurbriggen, and M. Ordonez, "Dual-loop geometric-based control of full-bridge inverters for stand-alone distributed generation systems," in *2016 IEEE 7th International Symposium on Power Electronics for Distributed Generation Systems (PEDG)*, June 2016, pp. 1–5.

[35] F. Paz and M. Ordonez, "High-accuracy impedance detection to improve transient stability in microgrids," *IEEE Transactions on Industrial Electronics*, vol. 64, no. 10, pp. 8167–8176, Oct 2017.

[36] A. M. Rahimi, G. A. Williamson, and A. Emadi, "Loop-cancellation technique: A novel nonlinear feedback to overcome the destabilizing effect of constant-power loads," *IEEE Transactions on Vehicular Technology*, vol. 59, no. 2, pp. 650–661, Feb 2010.

[37] G. Sulligoi, D. Bosich, G. Giadrossi, L. Zhu, M. Cupelli, and A. Monti, "Multiconverter medium voltage dc power systems on ships: Constant-power loads instability solution using linearization via state feedback control," *IEEE Transactions on Smart Grid*, vol. 5, no. 5, pp. 2543–2552, Sept 2014.

[38] J. A. Solsona, S. G. Jorge, and C. A. Busada, "Nonlinear control of a buck converter which feeds a constant power load," *IEEE Transactions on Power Electronics*, vol. 30, no. 12, pp. 7193–7201, Dec 2015.

[39] Q. Xu, C. Zhang, C. Wen, and P. Wang, "A novel composite nonlinear controller for stabilization of constant power load in dc microgrid," *IEEE Transactions on Smart Grid*, vol. PP, no. 99, pp. 1–1, 2017.

[40] I. G. Zurbriggen, M. Ordonez, and M. Anun, "Dynamic physical limits of buck converters: The t0/4 transient benchmark rule," in *2013 Twenty-Eighth Annual IEEE Applied Power Electronics Conference and Exposition (APEC)*, March 2013, pp. 421–428.

[41] Y. Zhao, W. Qiao, and D. Ha, "A sliding-mode duty-ratio controller for dc/dc buck converters with constant power loads," *IEEE Transactions on Industry Applications*, vol. 50, no. 2, pp. 1448–1458, March 2014.

[42] C. N. Onwuchekwa and A. Kwasinski, "Analysis of boundary control for buck converters with instantaneous constant-power loads," *IEEE Transactions on Power Electronics*, vol. 25, no. 8, pp. 2018–2032, Aug 2010.

[43] M. Ordonez, M. Iqbal, and J. Quaicoe, "Selection of a curved switching surface for buck converters," *IEEE Trans. Power Electron.*, vol. 21, no. 4, pp. 1148–1153, 2006.

[44] W. Burns and T. Wilson, "A state-trajectory control law for DC-to-DC converters," *IEEE Trans. Aerosp. Electron. Syst.*, vol. AES-14, no. 1, pp. 2–20, 1978.

[45] M. Anun, M. Ordonez, I. Zurbriggen, and G. Oggier, "Circular switching surface technique: High-performance constant power load stabilization for electric vehicle systems," *Power Electronics, IEEE Transactions on*, vol. 30, no. 8, pp. 4560–4572, Aug 2015.

[46] R. W. Erickson and D. Maksimović, "Fundamentals of power electronics." Kluwer Academic Publishers, 2004, ch. 9.

[47] S. Buso and P. Mattavelli, *Digital control in power electronics.* Morgan and Claypool, 2006.

[48] B. T. Irving and M. M. Jovanovic, "Analysis, design, and performance evaluation of droop current-sharing method," in *APEC 2000. Fifteenth Annual IEEE Applied Power Electronics Conference and Exposition (Cat. No.00CH37058)*, vol. 1, 2000, pp. 235–241 vol.1.